UNIVERSITÀ
DEGLI STUDI
DI PADOVA

UNIVERSITA' DEGLI STUDI DI PADOVA

Dipartimento di Ingegneria Industriale DII

Corso di Laurea Magistrale in Chemical and Process Engineering

Design of an Integrated Energy System using a Cascade High Temperature Heat Pump with Zeotropic Refrigerants.

Relatore

Dr. Federico d'Amore

Correlatore

Dr. Prof. Trygve M. Eikevik

Laureando

Omar Volpato 2041548

Anno Accademico 2024/2025

Abstract

This thesis deals with the design and modelling of an integrated energy system capable of sustaining its operation. This system is based on a cascade high-temperature heat pump utilizing zeotropic refrigerants. The heat pump design is specifically sized to generate hot water for district heating with a Coefficient of Performance (COP) of 3.6. This system is modelled in Matlab and tested on the geographic area of Oslo as a case study. The simulation is performed over a year on an hourly basis. The system provides enough heat to satisfy the district heating demand for 9/12 months of the year while also achieving self-sustainability during its operation. In addition, the deployment of zeotropic mixtures as refrigerants adds an extra layer of efficiency and adaptability to the system thanks to their temperature glide. The results highlight that the proposed system not only meets the design specifications, but it is also a sustainable and efficient source of energy. Overall, the work demonstrates the good potential of high temperature heat pumps to effectively address the energy needs of residential communities.

Sommario

Questa tesi tratta la progettazione e modellazione di un sistema energetico integrato in grado di sostenere la sua operazione. Il sistema è basato su una pompa di calore ad alta temperatura a cascata che utilizza refrigeranti zeotropici. Il progetto è dimensionato specificatamente per generare acqua calda per il riscaldamento urbano con un Coefficiente di Prestazione (COP) che supera 3.6. Questo sistema è modellato con Matlab e testato nell'area geografica di Oslo come caso studio. La simulazione è eseguita durante un intero anno su base oraria. Il sistema fornisce abbastanza calore da soddisfare la domanda di riscaldamento urbano per 9/12 mesi, garantendo contemporaneamente l'autosufficienza energetica durante il suo funzionamento. Inoltre, l'impiego di miscele zeotropiche come refrigeranti aggiunge un ulteriore strato di efficienza e adattabilità al sistema, grazie al loro *temperature glide*. I risultati evidenziano che il sistema proposto non solo soddisfa le specifiche di processo, ma è anche una fonte di energia sostenibile ed efficiente. Complessivamente, questo lavoro dimostra l'alto potenziale delle pompe di calore ad alta temperatura nell'affrontare in modo efficace le esigenze energetiche delle comunità residenziali.

Preface

Embarking on an academic journey often takes unexpected turns, and mine led me to the enriching experience of Erasmus+ mobility. As I stand at the completion of this thesis, I am filled with gratitude for the unique opportunities and perspectives that this international adventure has provided. I acknowledge the University of Padova for granting me the opportunity to participate in the Erasmus+ program. This experience has not only broadened my academic horizons but has also enriched my personal and professional development in ways I could have never imagined. I am deeply grateful to my UniPd supervisor Federico d'Amore for his unfaltering support and guidance across this journey. I would like to express my gratitude to my esteemed supervisor at NTNU, Trygve M. Eikevik and co-supervisor postdoctoral fellow, Ganesan Palanichamy. Your insightful mentorship, and boundless patience have been instrumental in shaping this research, even across borders.

After my semester abroad at NTNU I would like to thank my family, always supporting me from home, being my steadfast pillars of strength through challenges and triumphs. I am also profoundly grateful to my ex-housemates who generously dedicated their time to correct and revise my work. Your willingness to engage in scholarly discourse, despite the non-academic nature of our living arrangements, has been invaluable. In closing, I dedicate this work to those who have accompanied me on this long journey, you are an integral part of it. My hope is that this thesis will contribute, in some small measure, to the ever-expanding mosaic of knowledge.

Omar Volpato

Università degli Studi di Padova (UniPd)

Norges Teknisk-Naturvitenskapelige Universitet (NTNU)

22/02/2024

Table of Contents

List of Figures

List of Tables

List of Abbreviations

AHX	Auxiliary Heat Exchanger
ASHRAE	American Society of Heating, Refrigerating and Air Conditioning Engineering
BFD	Block Flow Diagram
BHE	Borehole Heat Exchanger
BTES	Borehole Thermal Energy Storage
CFC	ChloroFluoroCarbon
CO_2	Carbon Dioxide
COP	Coefficient of Performance
DH	District Heating
GSHP	Ground Source Heat Pump
HFC	HydroFluoroCarbon
HP	Heat Pump
HS	High Stage
HT	High Temperature
HTHP	High Temperature Heat Pump
HX	Heat Exchanger
IES	Integrated Energy System
IHX	Internal Heat Exchanger
ISO	International Organization for Standardization
LDC	Load-Duration Curve
LMTD	Logarithmic Mean Temperature Difference
LS	Low Stage
LT	Low Temperature
NIST	National Institute of Standard and Technology
NTNU	Norges Teknisk-Naturvitenskapelige Universitet
ODP	Ozone Depletion Potential
PCM	Phase-Change Material
PCM-TES	Phase-Change Material Thermal Energy Storage

PFD	Process Flow Diagram
PV	PhotoVoltaic
PVT	PhotoVoltaic/Thermal
RTE	Round-Trip Efficiency
SAHP	Solar Assisted Heat Pump
SDG	Sustainable Development Goals
TCM	Thermo-Chemical Materials
TES	Thermal Energy Storage
VHTHP	Very High Temperature Heat Pump
VLE	Vapor-Liquid Equilibrium

Nomenclature

A	Area [m^2]
B	Battery capacity [kWh]
c_p	Specific heat capacity [kJ/(kg*K)]
COP	Coefficient of performance [-]
D	Heat demand [kW]
E	Error on the LMTD [K]
h	Enthalpy [kJ/kg]
H	BTES capacity [kWh]
I_t	Solar irradiance [W/m^2]
$\dot{m}$	Mass flow rate [kg/s]
P	Pressure [bar]/[kPa]
$\dot{P}_{el}$	Electrical power from PVT [kW]
$\dot{P}_{th}$	Thermal power from PVT [kW]
$\dot{Q}$	Heat flow [kW]
r	Compression ratio [-]
s	Entropy [kJ/(kg*K)]
S	PCM-TES capacity [kWh]
T	Temperature [K]/[°C]
T_a	Air temperature [K]/[°C]
U	Global heat transfer coefficient [$W/(m^2*K)$]
V_c	Compressor size [m^3/h]
$\dot{W}$	Work flow [kW]
ΔT_{ml}	Logarithmic mean temperature difference [K]
η	Efficiency [-]
θ	Temperature difference [K]
ρ	Mass density [kg/m^3]

Executive Summary

Introduction

The global energy demand has risen by 15% in the last decade. Sustainable solutions are essential to meet this increasing need, aligning with global initiatives like the Sustainable Development Goals. This thesis addresses the crucial task of designing and modeling an integrated energy system. Heat pumps offer an alternative to traditional heating systems, extracting and transferring heat to reduce greenhouse gas emissions. Zeotropic mixtures enhance energy efficiency of the system, while the integration of renewable energy sources with the heat pump contributes to the reduction of the environmental impact. The proposed IES includes a core HTHP with zeotropic refrigerants, powered by PVT panels and aided by energy storages to produce hot water for district heating.

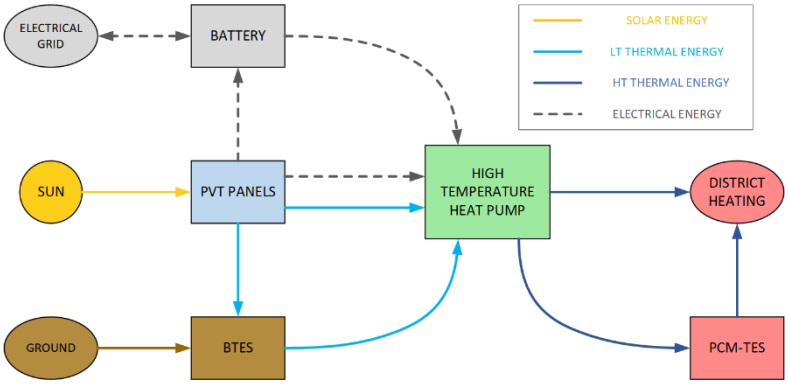

Methodology

The integrated energy system is simulated throughout the year using Matlab. Each section of the system is modelled independently, the models are then merged to describe the overall network operation. The base location for building the system is the city of Oslo, historical meteorological data are used to predict the heat demand for district heating and regulate the heat production. The heat pump is sized with respect to the total amount of heat to be delivered and the zeotropic refrigerants are selected based on their thermodynamic properties. Finally, using energy integration, the energy-efficiency of the heat pump is maximized.

Results

The way in which the heat pump is operated varies significantly between summer and winter. In winter, due to the reduced energy production by the PVT panels, the importation

of electricity from the external grid is frequent and often the heat pump operates at partial load. Conversely during summer, it can always operate at full capacity and, since the heat demand is usually low, the heat pump can also be switched-off, supplying the heat stored in the TES. Overall, a positive balance between exporting and importing electrical energy from the grid demonstrates that the system can sustain its operation, but it cannot be independent, particularly in winter. The use of a high-efficiency battery storage allows to reduce the energy importation.

Conclusions

The design of an integrated energy system comprising a high temperature heat pump was possible. Zeotropic mixtures used as refrigerants in the heat pump ensure the perfect temperature match between fluids in the heat exchangers, boosting the energy efficiency. The simulation of the IES throughout the year using Matlab showed good results: the heat pump produces hot water at 100°C for district heating, achieving a COP of 3.6. The IES sustains operation, thanks to the synergic action of its sections, also generating a surplus power in summer. The integration of cascade HTHPs in an IES appears to be a promising avenue for sustainable and efficient energy utilization.

1. Introduction

1.1. Background and Motivation

The world has been witnessing an unprecedented surge in the demand of energy prompted by rapid population growth, industrialization and technological progress. The total world energy production is increased of 15% in the last 10 years, with an increase of 11% in the demand for residential use [1]. The investigation and development of sustainable and efficient solutions have become of primary importance to face this escalating need for energy. In the prospect of energy systems, the alignment with global initiatives such as the Sustainable Development Goals (SDGs) is now more pressing than ever. The SDGs are 17 interlinked objectives focusing on the environmental, social and economic aspects of sustainable development [2]. This thesis explores the possibility of building an integrated energy system with a particular emphasis on key SDGs, such as affordable and clean energy (SDG 7), industry, innovation, and infrastructure (SDG 9), and climate action (SDG 13). In the past decades, the use of fossil fuels for heating purposes has been the predominant solution worldwide. In the Net Zero Emissions by 2050 scenario set by the European Union [3], in line with the global climate action under the Paris Agreement [4], the use of green energy source must become the preferred choice for a substantial reduction of CO_2 emissions in the atmosphere.

Heat pumps offer an energy-efficient alternative to traditional heat generation, with reduced greenhouse gas release. A heat pump is an energy system that extracts heat from a source, amplifies and transfers it to where is needed. Industrial processes that require heating and waste heat disposal can benefit from the development of high temperature heat pumps. The investment cost of boilers and cooling towers can be potentially saved with a single more efficient and less complex energy system, at the same time reducing the environmental footprint. Furthermore, zeotropic mixtures can be used as refrigerants in heat pumps. These mixtures are blends of substances with different boiling points; based on the composition, the thermodynamic properties of the mixture change. The employment of zeotropic refrigerants adds a layer of complexity and innovation to the conventional heat pump paradigm, enhancing the energy-efficiency.

A heat pump can be implemented within an integrated energy system, as it requires both heat and electricity sources. Solar, ground, wind or hydropower are examples of

renewable energy sources that can be integrated to support the heat pump operation. Understanding and optimizing the interactions within the resulting IES becomes crucial as it directly contributes to SDG 13. A simple block diagram representing the integrated energy system is reported in Figure 1. The HTHP is the core of the plant, it receives electricity and heat converted from solar energy by the PVT panels, then it delivers thermal energy as hot water to the district heating section. Three energy storage systems, namely a battery, one or more boreholes and a phase-change material storage are used for maintaining a seasonal energy reserve. The boreholes can also extract heat from the ground, while the battery is connected to the electrical grid to import or export electrical energy when needed.

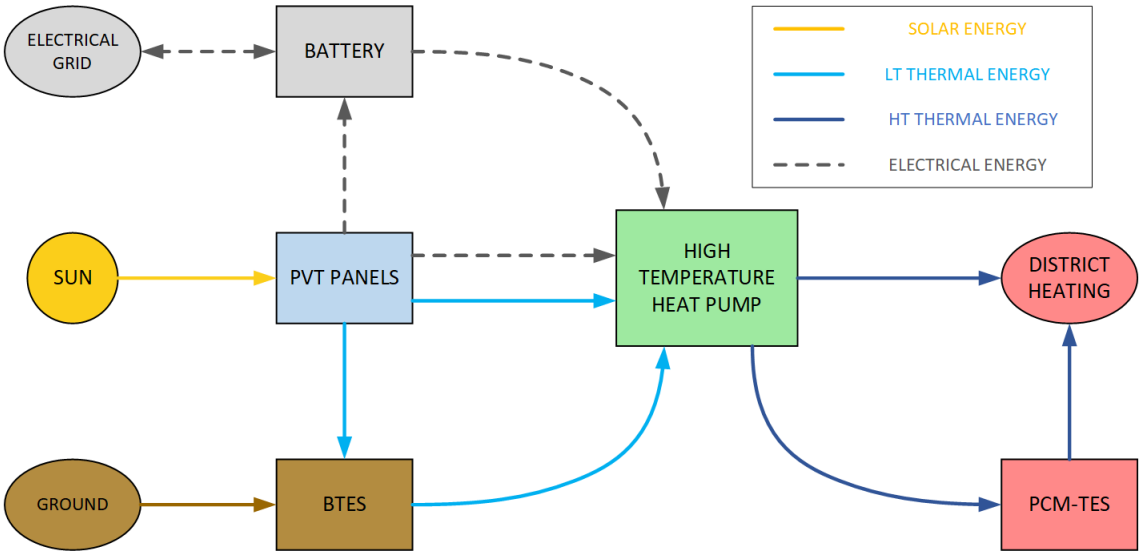

Figure 1: BFD of the integrated energy system.

1.2. About the Project

This work is part of the bigger project "Key technologies and demonstration of combined cooling, heating and power generation for low-carbon neighborhoods/buildings with clean energy" (ChiNoZEN) [5]. The project is the result of the cooperation of Norwegian and Chinese researchers within energy topics. The ChiNoZEN project supports the transition to a reliable, affordable, publicly accepted and sustainably built environment, aiming at reducing fossil fuel dependency in the face of increasingly scarce resources, growing energy needs, and threatening climate change. The project delivers new knowledge, solutions and innovative technologies for low-carbon buildings and

neighborhoods. The key result of the ChiNoZEN project is a combined cooling, heating and power generation system able to meet the needs of low-carbon communities to fully absorb nearby available renewable energy. The project is funded by the Research Council of Norway and the Ministry of Science and Technology in China, and has a variety of industry and academic partners in China and Norway (NTNU Department of Energy and Process Engineering, 2020).

Previous research works on the high temperature heat pump field are used as a starting point for this thesis. Many concepts and parameters for modelling the plant are taken from the master's theses written by Ryssdal [6] and Skoglund [7] and from Ganesan's publications on high temperature heat pumps with zeotropic refrigerants [8] [9].

1.3. Objectives

The main objective of this study is to integrate a high temperature heat pump into an energy system, to satisfy the energy demand of residential buildings along the whole year. The performance of the system is tested through a Matlab simulation under varying conditions of a real-world scenario based in Oslo. The design aims to obtain a simple system configuration, maximizing the energy efficiency, while at the same time achieving self-sustainability. The use of zeotropic fluids represents an innovative solution in the refrigeration field, and can bring significant improvements in the results. The project also considers the integration of photovoltaic/thermal panels and boreholes for supplying thermal energy to the heat pump. A major goal is therefore to fill literature gaps about solar-assisted and ground-assisted heat pumps. Highlighting the potential of high temperature heat pumps in contributing to clean and sustainable energy solutions through the results is the final target of the project.

1.4. Chapter summary

A brief overview of the chapters structure is now provided.

- Literature review: previous researches in the heat pump field are presented divided in specific subsections.

- Theory: theoretical details about heat pumps, photovoltaic panels and thermal energy storages.
- Simulation approach: technical details of the design and simulation of all the subsystems and of the overall integrated energy system.
- Results: outcome of the simulation displayed in graphs and tables for the whole year and for different seasons.
- Discussion: critical examination of sizing, simulation and results, with comparisons between different operation periods.
- Conclusions: final summary of the work done based on the discussion of results, with proposals of further research.

2. Literature Review

Prior to the design and simulation of the integrated energy system, a literature review is drawn up. It is composed of relevant research papers and patents on the existing heat pump technology, with a focus on the implementation of zeotropic refrigerants and solar/ground heat sources. The review is divided into specific sections.

2.1. Heat Pumps

A patent for an optimized heat pump system was granted to Slack and his collaborators in 2017 [10]. They designed a system for space heating or cooling including a heat pump with a refrigeration circuit for transferring heat between a source and a sink for heating and cooling operations. An interface receives user inputs, including an indication of discomfort based on temperature. The controller creates a profile for a minimum and a maximum comfortable temperature level, and controls the heat pump to perform heating and cooling operations in accordance with the profiles for comfortable temperature levels. The controller may also generate an optimized heat demand plan in accordance with predictions of outdoor and indoor temperature, cost, and demand. The plan is then optimized to cost-effectively maintain the temperature of the heated space within the comfortable temperature range defined by the profiles.

Olympios et al. [11] presented a methodology for identifying optimal designs for a low-temperature air-source heat pump with a single-stage compressor, based on the vapor-compression cycle suitable for domestic heating applications. They accounted explicitly for a trade-off between cost and efficiency, as well as for the influence of the outside air temperature during off-design operation. This was achieved through the development of comprehensive design and off-design heat-pump models, composed of dedicated heat exchanger models, screw compressor efficiency maps and costing correlations. Cost and performance of twelve different heat pump configurations with the same heat output were explicitly captured. The possible heat pump designs were integrated into a whole-energy system model representing the UK electricity and heat system, allowing the best configuration to be identified. The results showed that the best design and off-design performance was ensured using refrigerants R-152a and R-410a. From a system perspective, high-performance heat pumps require significantly less installed electricity generation capacity (20 GW) to decarbonize domestic heat by 2050, and therefore

produce lower and more realistic power grid expansion rates. However, the use of a larger heat exchanger does not compensate overall for the increased technology cost, with low-performance HP being associated with the lowest system transition cost, which is about £35 billion lower than that achieved by higher-performance units. In their future work, Olympios et al. will consider more working fluid and component sizes, which will require the use of sophisticated surrogate models suitable for integrating the heat pump optimization problem within the whole-energy system optimization model.

2.2. High Temperature Heat Pumps

Hays' design for a high temperature heat pump (2002) has been influential in the field [12]. The invention relates generally to the utilization of waste heat in industrial applications, and in buildings, and more particularly the use of heat pumps to enable such low-level (<200°F) waste heat utilization, which is enormous. Basically, the invention is embodied in heat pump apparatus comprising a low temperature heat exchanger to produce vapor of a first fluid with the heat transferred from a second fluid, a high temperature heat exchanger to heat the second fluid to useful high temperatures from the condensation of the first fluid. A compressor increases pressure and temperature of the vapor, while an expansion valve lowers pressure and temperature of the first fluid producing a mixture of vapor and liquid.

Bamibegtan et al. [13] conducted a theoretical analysis to evaluate available and potential fluids with thermodynamic properties that are applicable for HTHPs. They showed that certain hydrocarbons and halocarbons are the most promising fluid candidates for waste heat upgrade from low to high temperatures, up to 125°C. The restrictions of safety and environmental impacts imposed by the Kigali's amendment to the Montreal protocol were considered. From the study resulted that R-600 and R-1233zd(E), show the highest potential for the immediate future implementation in HTHPs. R-600, though with lower COP compared to the heavier hydrocarbons, has a broad operating range and is therefore more flexible for different operating conditions. Also it is thermodynamically closer to R-600a and R-290 which have well developed compressor technology, and can be used directly in these compressors with little modifications. On the other hand, R-1233zd(E) showed a high COP with favorable autoignition temperature compared to R-601;

nevertheless, its stability and compatibility must be tested and verified at the operating conditions, since its decomposition products are highly toxic and have negative effects on the environment. In their further research, Bamigbetan et al. will include experimental verification of the performances of the simulated fluids via laboratory scale tests, to obtain a better understanding of the fluids in operation at high temperature during compression. Furthermore, they will investigate the impact of fluid dependent effects like pressure drop, lubrication compatibility and lubrication stability on the process.

Urbanucci et al. [14] investigated the integration of high-temperature heat pumps within a trigeneration system. Hot water at around 90°C is produced with a heat pump using the waste heat from the condenser of the absorption chiller. Depending on the case, the cooling tower or the air cooler can be substituted. The technical applicability of current heat pump technology was assessed through a numerical model of the heat pump cycle, also testing the performance of different working fluids and the possibility to implement internal heat exchangers. An exergy analysis showed the advantages for energy production of the novel trigeneration system compared to traditional systems; the COP of the heat pump cycle was found a crucial parameter for the exergy performance. The economic feasibility of the proposed energy system was evaluated using a levelized cost of electricity methodology. The results indicated that incorporating a high-temperature heat pump in a trigeneration system could be economically advantageous when compared to traditional technologies. As part of a case study, Urbanucci et al. integrated this proposed trigeneration system into an already established separate-production plant at a pharmaceutical factory. The profitability was investigated through the economic optimization of the investment with a two-level algorithm. The adopted system allows around huge global cost saving: 40% with respect to separate energy production and 10% with respect to traditional cogeneration and trigeneration processes, providing also the flexibility to cover variable energy demands.

2.3. Cascade Heat Pumps

A design for a cascade heat pump system and with control system was developed by Choi (2011) [15]. A cascade type heat pump system was provided to immediately generate high temperature water for heating, or supplying it to maximize spatial utilization as separate

water heating equipment is not necessary. The cascade heat pump system includes a first heat pump unit, a second heat pump unit, a cooling-and-heating unit, and a hot water supplying unit. The cooling-and-heating unit includes a heat storage tank and a second fluid line for cooling and heating.

Yerdesh et al. [16] studied the application of a two-stage cascade heat pump cycle operating with two different refrigerants to provide a sustainable solution to lift the condenser temperature above 70°C. They made this study because both heating capacity and coefficient of performance of a single stage vapor compression heat pump cycle are significantly reduced at low temperatures. Many refrigerant pairs were numerically tested for low and high temperature cycles, using Engineering Equation Solver software for the calculation of thermal performance. R-32/R-134a and R-410A/R-134a showed the highest vapor compression cycle COP of 1.98, from -30°C ambient air temperature and +60°C heating circuit temperature range. The above-mentioned refrigerants will be eventually suppressed in near future by Paris Agreement. R-32/R-290 and R-744/R-290 working fluids combinations were proposed as environmentally friendly alternative in the cascade cycle; they also allow the compressors to operate at a lower pressure ratio. Yerdesh et al. made some proposals for further work, including a cascade system optimal operation control algorithm, cascade heat pump components and overall system thermodynamic optimization, a study of intermediate cascade heat exchanger operational conditions, and an energy and exergy study.

Jung et al. [17] investigated experimentally cascade multi-functional heat pump, combining a heat pump using R-410A for air heating with a water heating unit using R-134a for hot water supply. The results were compared with those of a single-stage multi-functional heat pump using R-410A for air and water heating. The performance of the cascade multi-functional heat pump was measured by varying the refrigerant charge amount, valve opening, water flow rate, and water inlet temperature. The adoption of the water heating unit in the cascade multi-functional heat pump showed more stable air and water heating operations, and yielded higher water outlet temperatures, up to 76.6°C (at the water inlet temperature of 40°C and water flow rate of 120 kg/h). The air heating capacity of the cascade multi-functional heat pump remained relatively constant even with variations of the water inlet temperature and water flow rate, while that of the single-stage multi-functional heat pump varied significantly. On the other hand, when the water

temperature was lower than 45°C, the COP of the cascade multi-functional heat pump was lower than the single-stage multi-functional heat pump.

Boahen and Choi [18] proposed a new cycle to enhance performance of the cascade heat pump by adopting an auxiliary heat exchanger (AHX) in desuperheater, heater and parallel positions at the low stage (LS) side. Compared to the conventional cycle, heating capacity and coefficient of performance (COP) of the new cascade cycle with AHX in desuperheater position increased up to 7.4% and 14.9% respectively. This strong improvement is due to the higher heat transfer to secondary fluid of the HS cycle in the AHX, and lowest pressure difference of the LS cycle.

2.4. Zeotropic Heat Pumps

Yilmaz [19] presented the performance analysis of an air-to-water vapor compression heat pump system using pure refrigerants and zeotropic refrigerant mixtures. The considered heat pump system was composed of compressor, condenser, air cooled evaporator, expansion valve, receiver tank, superheater/subcooler, refrigerant mixture unit and some auxiliary and measurement devices. Comparisons were made between the pure refrigerants R-12, R-22, R-114 and refrigerant mixtures R-12/R-114, R-12/R-22 based on the COP and second law efficiency; the effect of the evaporator source inlet temperature was also presented. Yilmaz concluded from his study that COP and second law efficiency increase with increasing evaporator source inlet temperature for both pure refrigerants and refrigerant mixtures; the results for pure refrigerants can be improved by using appropriate mixtures of the refrigerants. Moreover, the mixture ratio affects significantly the COP and second law efficiency of heat pumps, and this last factor can be used to identify the highest efficiency mixtures of refrigerants.

Navarro-Esbrí et al. [20] presented a semi-empirical assessment of a two-stage cascade cycle for high temperature heat pumps applications to produce hot water up to 150°C from a water flow at 35°C and 25°C. They assessed the energy performance of a cascade system through a validated semi-empirical model, considering several novel mixtures for both stages. The experimental results from two single-stage heat pump prototypes (R-1234ze(E) and R-1336mzz(Z)) with different temperature lifts were used for this study. The best refrigerant combinations, ensuring up to 14% COP increase respect to the base

experimental results, were R-152a/600 (0.08/0.92) and R-1233zd(E)/161 (0.88/0.12) for the low stage and high stage, respectively. While the LS mixture is highly flammable, a potential alternative that addresses flammability concerns is R-1234ze(E)/R-32 (0.7/0.3). Although the replacement exhibits a lower COP compared to the initial proposed combination, it still surpasses the baseline COP. The COP enhancement observed in the suggested mixtures is noteworthy but not excellent; however, the increase in the volumetric heating capacity reaches up to 30%. Future studies must consider different structures for obtaining better results in terms of efficiency.

2.5. Solar/Ground-assisted Heat Pumps

Sezen and Gungor [21] reviewed 77 recent studies on solar-assisted heat pump (SAHP) systems, which have been a popular research topic in last decades because of their proven improved performance by integrating solar energy to system. In their work, Sezen and Gungor organized systems based on their configurations, establishing a framework for comparison in their research. They explored how solar radiation and ambient temperature impact the performance of SAHP systems, identifying optimal ambient conditions for each system. The complexity of systems was gauged by the type and number of components employed, and costs analysis, factoring in the payback period, was conducted. The findings from the literature review indicated that, when solar irradiation is below 400 W/m^2, direct expansion systems are preferred due to their simultaneous use of solar energy and air as heat sources. Indirect expansion systems, while more complex, can be simplified by replacing the solar-side evaporator with a solar air preheater, effectively integrating the existing solar system and air source heat pump system. Additionally, the hindrance of temperature rise in indirect systems, preventing the use of PVT panels, can be overcome with low-cost external cooling devices.

Olabi et al. [22] investigated the advancements, applications, research trends related to ground source heat pumps (GSHPs), and the challenges and barriers that face their development based on a bibliometric analysis. The results showed that in recent years, a considerable growth in GSHP's research has been recognized, with a focus on heating more than cooling, because GSHP is more suitable for cold regions. Moreover, GSHPs can play a significant role in achieving the sustainable development goals (SDGs),

particularly for affordable and clean energy (SDG 7) and climate action (SDG 13). Based on the interpretation of the bibliometric analysis, Olabi et al. deduced that most of the challenges and barriers to GSHPs are related to their capital cost, groundwater contamination, regulations, subsidies, and incentives. An important point to clarify is that GSHP systems are highly sophisticated; as a result, installation, maintenance, and repair of these systems need the assistance of trained professionals. GSHPs however can create several jobs: engineers and designers for system design and installation, technicians for installation and maintenance, marketing personnel to promote GSHPs, researchers and scientists to develop the technology, and project managers to oversee installation and commissioning. Recent advancements in GSHPs are focusing on the development of new materials and designs to increase the efficiency of heat transfer from/to the ground/heat pump; this can lead to smaller GSHP systems that use less energy and are more cost-effective.

Lazzarin and Noro [23] studied the performance of a PVT dual source heat pump, operating with the ground as source/sink in a refurbished building located in Northern Italy. Dual or multisource heat pumps were designed to address the limitations of single-source systems, such as outside air, water, ground, or solar radiation. In the case of solar radiation, incorporating Photovoltaic/Thermal (PVT) modules serves a dual purpose: recovering otherwise lost heat and enhancing the electrical efficiency of the PV system through cooling. The utilization of glazed PVT further improves the thermal efficiency of the collector. Additionally, coupling the system with the ground allows to maintain high electrical efficiency without risking damage to the cells due to overheating. During periods when the heat pump does not require heat or is operating for summer air conditioning, the ground serves as the heat sink for both the heat pump and PVT cooling. Lazzarin and Noro designed the plant by means of dynamic simulation considering five alternatives with increasing solar field area (20-40-60 m^2) and decreasing number of boreholes (5-4-3 of 100 m each), and compared them with a traditional solution (NG boiler + air/water chiller). The most efficient solution was the alternative comprising a 60 m^2 PVT + 300 m boreholes. Expanding the solar field up to a certain threshold allowed for a reduction in the ground field extension, resulting in improved performance and reduced costs. This finding aligns with the conclusion drawn in earlier studies by different

authors. The overall plant demonstrates very high efficiency and low primary energy consumption, attributed in part to its substantial energy independency from the grid.

2.6. Literature summary

From the literature analysis it emerges that several studies have been done in the heat pump field. More specifically the selection of system design and of the best refrigerant are problems investigated frequently. Olympios et al. [11] created an optimization model that can find the most suitable HP design alternative as a trade-off between performances and costs. They integrated the different designs in a real-world scenario including many external factors. Bamigbetan et al. [13] studied the performance of many different fluids with low ODP for future applications to HTHPs. They discovered that light hydrocarbons like R-600 (n-butane) can be used as refrigerants with a little modification of the existing plants. Additionally, the use of zeotropic refrigerants in heat pumps and the integration of heat pumps in IESs are often possibilities to be explored. Navarro-Esbrí et al. [20] compared the performance of zeotropic mixtures with different combinations of fluids in a prototype cascade HTHP. They observed an increase in both COP and heating capacity with respect to traditional refrigerants. Lazzarin and Noro [23] analyzed dual-source heat pumps, and discovered that coupling heat pump system with PVT panels and boreholes brings many advantages. They selected the best configuration of the IES, varying the extension of the PVT panels field and the number of boreholes. This thesis aims to cover all the above-mentioned research questions, it designs an integrated energy system with a cascade high temperature heat pump. Zeotropic mixtures are used as refrigerants, the most suitable compositions to maximize the performances are selected. The HTHP uses a solar/ground source with the integration of PVT panels and boreholes; it provides hot water for district heating and achieves a high energy efficiency in terms of COP.

3. Theory

In this chapter a theoretical description of the subsystems used for building the integrated energy system (IES) is given. Specifically, the principles governing cascade heat pump is extensively illustrated, together with a thermodynamic elucidation of the use of zeotropic refrigerants in the heat pump cycle. Furthermore, a basic description of the functioning of photovoltaic/thermal panels, thermal energy storage and borehole storage is provided in the next subsections.

3.1. Heat Pumps

Heat pumps are a promising technology for heating (and cooling) domestic buildings that provide exceptionally high thermal and electrical efficiencies compared with fossil fuel combustion [24]. The HP has evolved to become a mature technology over the past three decades. They use an external energy source, often electricity, to remove heat from a cold location called heat source and pump it to a warmer one called heat sink, by continuously circulating a refrigerant.

A heat source can be a gas, air, water (surface water, underground water or discharged hot water) or the ground; a heat sink can be space heating (radiant panels, warm air, convective systems, etc.) for low-temperature heating systems, or water heating for high temperature heating systems [25]. The main classification of HPs is related to the way in which external energy is driven into the system; a HP can use electrical energy (electro-

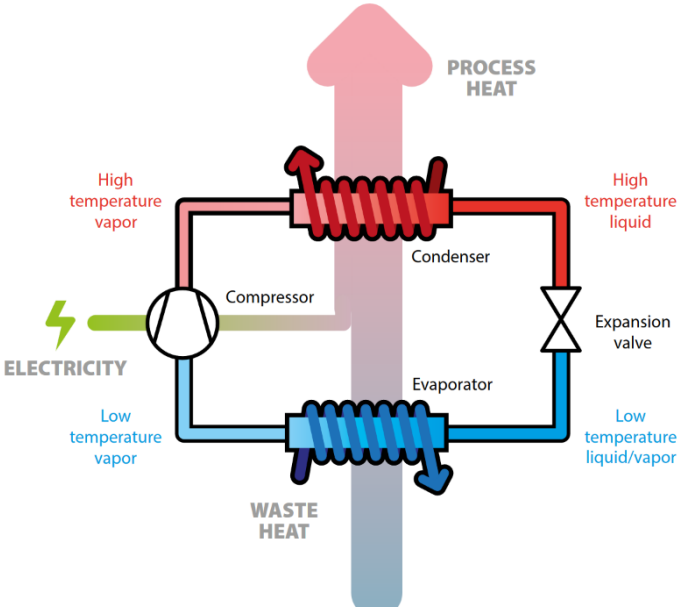

Figure 2: Scheme of a generic vapor compression heat pump.

compressor), mechanical energy (mechanical compression with expansion turbines), thermo-mechanical energy (steam ejector), thermal energy (absorption cycle), or thermo-electrical energy (Peltier effect). Most of the HPs used nowadays are based on a vapor-compression cycle, namely they are electrically driven; they include four basic units: an evaporator, a condenser, a compressor, and an expansion valve (see Figure 2 [26]).

A HP cycle can be visualized from a thermodynamic point of view in a temperature-entropy (T-s) diagram or in a pressure-enthalpy (P-h) diagram.

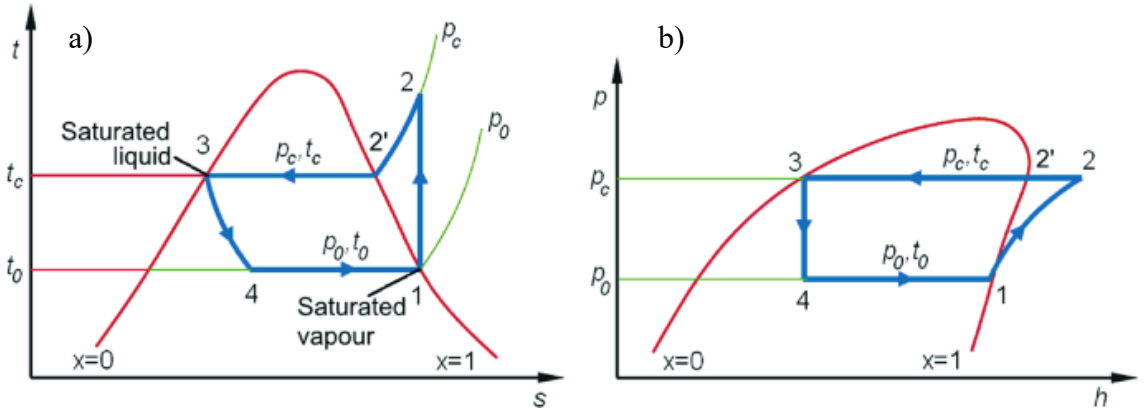

Figure 3: Temperature-entropy (T-s) diagram (**a**) and pressure-enthalpy (P-h) diagram (**b**) of the theoretical HP cycle.

The theoretical vapor-compression HP cycle, shown in Figure 3 [27], assumes isentropic compression, with no superheating of the vapor nor subcooling of the liquid; it is composed of the following reversible transformations of a closed system:

a) $(1 \rightarrow 2)$: Isentropic compression of the cold saturated vapor in the compressor, which increases pressure and temperature from (p_0, t_0) to (p_c, t_2).
b) $(2 \rightarrow 2')$: Isobaric cooling of the hot superheated vapor in the condenser at the pressure p_c, which reduces the temperature from t_2 to t_c.
c) $(2' \rightarrow 3)$: Isobaric condensation of the hot saturated vapor in the condenser at the pressure p_c.
d) $(3 \rightarrow 4)$: Isenthalpic expansion of the hot saturated liquid in the valve, which reduces pressure and temperature of the hot saturated liquid from (p_c, t_c) to (p_0, t_0).
e) $(4 \rightarrow 1)$: Isobaric evaporation of the biphasic fluid in the evaporator at the pressure p_0.

The specific compression work delivered to the system is given by Equation 3.1:

$$w = h_2 - h_1 \tag{3.1}$$

The specific heat gained by the system during the evaporation is given by Equation 3.2:

$$q_e = h_1 - h_4 \tag{3.2}$$

The specific heat lost by the system during the condensation is given by Equation 3.3:

$$q_c = h_2 - h_3 \tag{3.3}$$

Where the h_i represent the specific enthalpy of the fluid at the point i in the diagrams in Figure 3.

The efficiency of a HP cycle is usually represented in terms of the coefficient of performance (COP), which is defined as the ratio between the useful heat supplied by the system and the work supplied to the system; its definition is reported in Equation 3.4:

$$COP_{HP} = \frac{q_c}{w_c} > 1 \tag{3.4}$$

In the case of a real vapor-compression HP cycle, all the transformations are no longer reversible. The compression step is polytropic and pressure and heat losses are present in pipes and equipment; it is shown in Figure 4 [27].

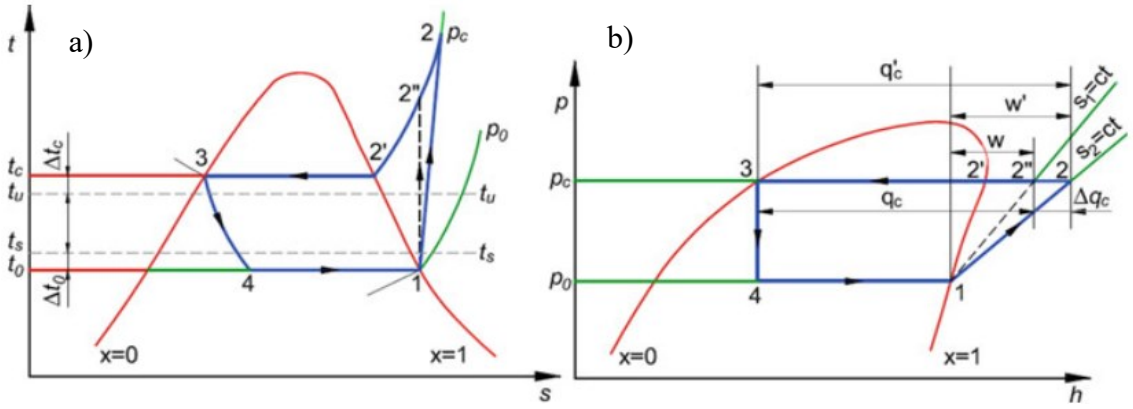

Figure 4: Temperature-entropy (T-s) diagram (**a**) and pressure-enthalpy (P-h) diagram (**b**) of the real HP cycle.

The isentropic efficiency of the compression step can be calculated according to Equation 3.5:

$$\eta_S = \frac{w}{w'} = \frac{w' - \Delta q_c}{w'} = 1 - \frac{\Delta q_c}{w'} < 1 \tag{3.5}$$

Where $w'$is the adiabatic irreversible compression work and Δq_c is the increase in the specific thermal load due to the non-ideality of the compression process. The real coefficient of performance of the HP system is therefore given by Equation 3.6:

$$COP'_{HP} = \frac{q'_c}{w'} = \frac{q_c + \Delta q_c}{w + \Delta q_c} = \frac{q_c + \left(\frac{1}{\eta_S} - 1\right) w}{w + \left(\frac{1}{\eta_S} - 1\right) w} = (COP_{HP} - 1)\eta_S + 1 < COP_{HP} \quad (3.6)$$

Where q'_c is the real specific thermal load of condensation in the real cycle. A real HP process has always a lower COP compared to the ideal case, which represents the upper limit of efficiency. In addition, the overall COP of the heating system is further diminished mainly because of mechanical and electrical losses of the compression equipment. Usually, the COP of a heat pump system ranges between 2 and 6.

3.2. High Temperature Heat Pumps

There is not a generally accepted temperature level to distinguish between high temperature heat pumps (HTHP) and regular heat pumps. A possible classification criterion, proposed by Arpagaus et al. [28]. It is based on the heat source and sink temperature levels: HTHPs have a source temperature between 40 and 60°C and a sink temperature between 80 and 100°C, if the temperature levels are higher, it is the case of a very high temperature heat pumps (VHTHP). This concept was presented by Bobelin et al. [29]. In this work no distinction will be made between HTHPs, and VHTHPs; their operations are in fact identical. The only difference between high temperature heat pumps and regular heat pumps is in the heat source delivery temperature, obviously higher for the former. HTHPs are extensively used in industry to remove waste heat at 30-70°C, a level significantly higher if compared to outdoor air, seawater, groundwater or geothermal heat.

3.3. Cascade Heat Pumps

Cascade heat pumps are used in many industrial applications when the temperature difference between heat source and heat sink is too high to ensure the transfer of heat with a satisfactory efficiency. In cascade systems two or more HP cycles are nested together by means of cascade heat exchangers (see Figure 5). In this way the compression ratio of each cycle is much lower than the total one, ensuring a higher compression efficiency.

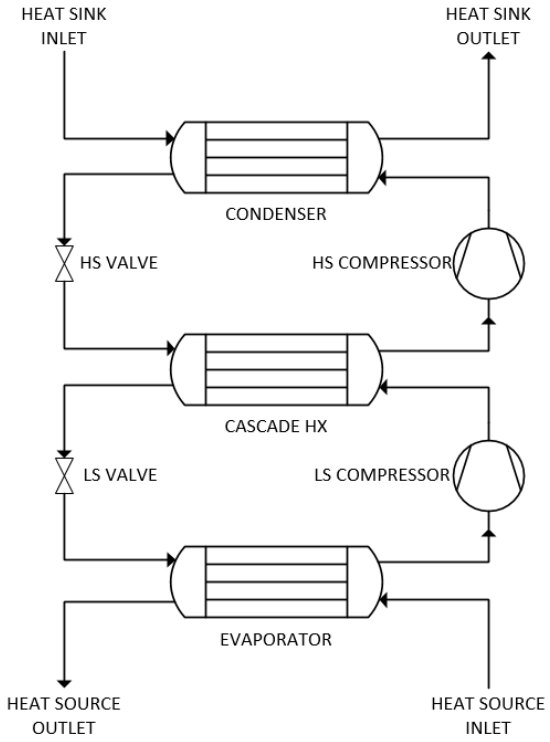

Figure 5: General scheme of a two-stage cascade HP.

The latent heat of vaporization of a refrigerant is lower at higher pressures, reaching zero at the critical point; therefore, the use of the same refrigerant for both high and low stages usually is not the optimal solution. The refrigerants used in a cascade HP have an increasing critical point by increasing the stage. The coefficient of performance for a cascade heat pump can be calculated according to Equation 3.7:

$$COP_{Cascade\ HP} = \frac{q_c}{\sum_i w_i} \tag{3.7}$$

Where w_i is the compression work in the i-th stage [27].

3.4. Zeotropic Mixtures

A zeotropic mixture (or non-azeotropic mixture) is a mixture of two or more substances with different boiling points. The boiling point of a zeotropic mixture at a given pressure and composition is not unique, but ranges between the bubble point and the dew point, therefore a temperature glide exists at every composition except for the pure components. When a liquid zeotropic mixture vaporizes, it produces the first bubble of gas at the bubble point and consumes the last drop of liquid at the dew point, vice-versa during condensation. An azeotropic mixture presents at least one composition, called azeotrope,

in which the bubble point and the dew point are equal, namely its temperature glide is zero, and it behaves as a pure refrigerant (see Figure 6).

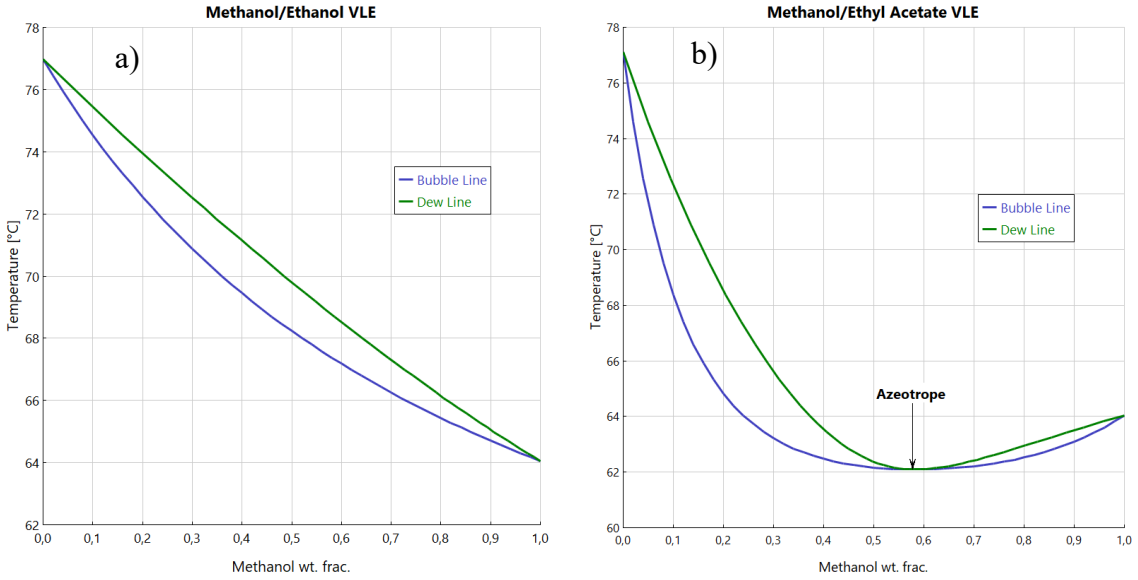

Figure 6: Example of VLE for a zeotropic mixture (**a**) and for an azeotropic mixture (**b**).

Usually, pure refrigerants are used as working fluids in heat pumps. In those cases the HP can be seen thermodynamically as a reversed Carnot cycle, made of two isothermal and two isentropic transformations. When a zeotropic mixture is used, the heat pump resembles a modified Lorentz cycle, made of an isothermal, an isobaric and two isentropic transformations (see Figure 7 [7]).

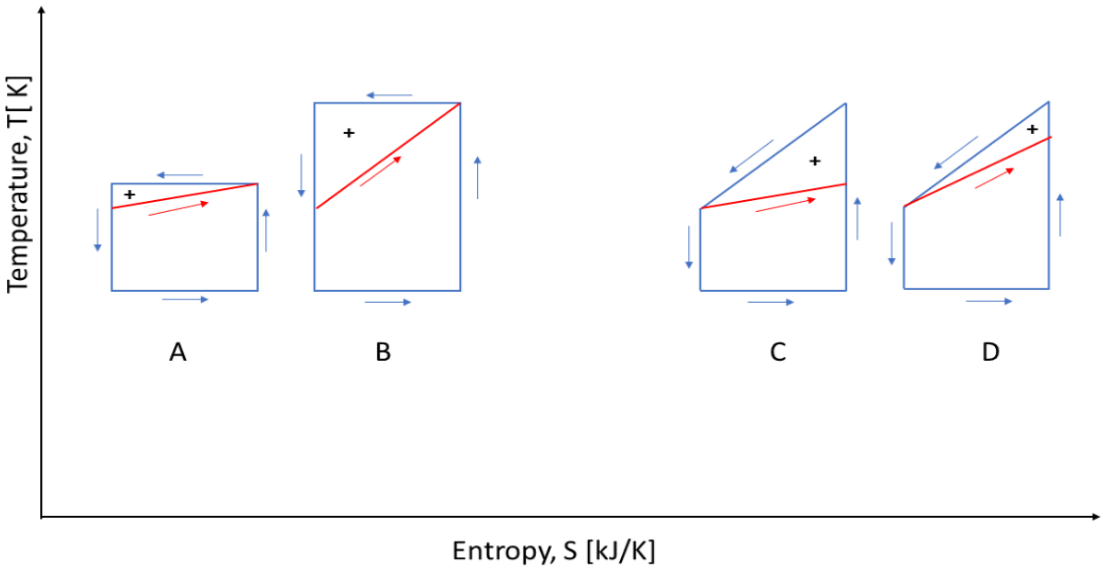

Figure 7: Sketch of the reverse Carnot cycle (left) and modified Lorentz cycle (right).

According to Stene [30], the modified Lorentz cycle has lower thermodynamic losses with respect to the reverse Carnot cycle, because of the better temperature profiles

coupling between refrigerant and the counterflow secondary fluid. In Figure 7 the energy loss is represented graphically by a + sign. It results in an optimal composition of the zeotropic mixture that can be found ensuring the best coupling with the secondary fluid, minimizing the energy losses.

3.5. Photovoltaic/Thermal Panels (PVT)

Solar energy is a renewable energy that derives from the sun's radiation. It is abundant and widely distributed on earth, it is available for the whole year without costs almost everywhere, and it is clean because it does not generate pollution. For these reasons, solar energy is nowadays considered as one of the most valuable alternatives to the use of fossil fuels. As the world's need for energy is continuously increasing, also the technology for collecting solar energy makes steady progress in increasing the efficiency and reducing the costs of these systems.

Photovoltaic panels (PV) can be used to convert the sun radiation into electrical energy. Their basic building block is the solar cell, these cells are connected to form a module, which are in turn arranged to form an array with a flat surface. Each cell is made by contacting two layers of semiconductor materials with opposite charges: a p-type positive layer (an intrinsic semiconductor doped with an electron-acceptor element) and a n-type negative layer (an intrinsic semiconductor doped with an electron-donor element) separated by a p-n junction as shown in Figure 8. When the cell is exposed to solar radiation, photons hitting the surface knock electrons loose, which then travel through a

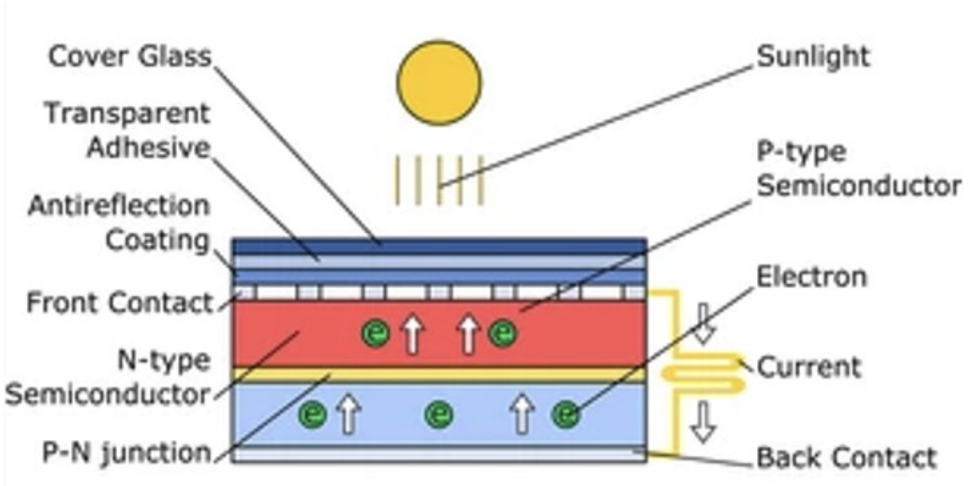

Figure 8: Simplified scheme of a solar cell.

circuit from one layer to the other, generating electricity. The surface of PV panels is usually coated by an anti-reflecting protective material, often tempered glass, which maximizes the amount of light absorbed by the cells, protecting them from the action of atmospheric agents.

The electrical power produced by a PV panel is given by Equation 3.8:

$$P_{el} = \eta_{el} I_t A_{PV} \tag{3.8}$$

Where I_t is the incident solar radiation, A_{PV} is the total area of the PV panel, and η_{el} is the electrical efficiency of the PV panel. The electrical efficiency is therefore defined as the fraction of the incident radiation energy that is converted into electrical energy by the solar cells (Equation 3.9).

$$\eta_{el} = \frac{P_{el}}{I_t A_{PV}} < 1 \tag{3.9}$$

The value of η_{el} is usually quite low, Dhilipan et al. [31] made a comparison of different types of solar cells; overall the efficiency is around 20%. Furthermore, the electrical efficiency is lower at higher temperatures of the PV module; the temperature of the solar cells can increase because of the external air temperature or due to the conversion of a part of the solar radiation into heat [32]. A common and unexpensive method employed to decrease the temperature of the cells is the forced air circulation. This is an efficient solution only when the air temperature is low enough to rapidly remove the heat generated.

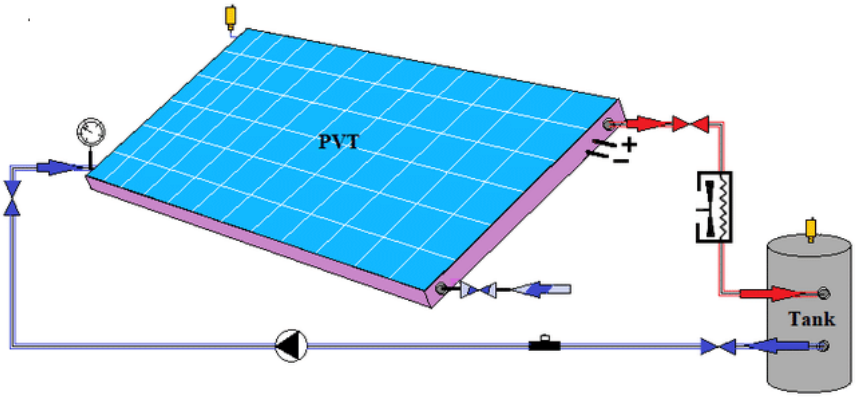

Figure 9: Simplified scheme of a photovoltaic/thermal (PVT) system.

When the air temperature is above 20°C for long periods of the year, which is common at low latitudes, the air heat removal works less effectively and the circulation of a refrigerant fluid is used instead [33]. The refrigerant, which usually is water, flows

through a heat exchanger in thermal contact with the rear part of the PV modules (see Figure 9). If the heat stored in the refrigerant fluid is used for heating purposes, then the system becomes a photovoltaic/thermal system (PVT), it offers a dual energy output and it can be effective in cost reduction [34].

The thermal power produced by a PVT panel is given by Equation 3.10:

$$P_{th} = \eta_{th} I_t A_{PVT} \tag{3.10}$$

Where A_{PVT} is the total area of the PVT panel and η_{th} is the thermal efficiency of the PVT panel. The thermal efficiency is therefore defined as the fraction of the incident radiation energy that is converted into heat by the solar/thermal system (Equation 3.11).

$$\eta_{el} = \frac{P_{th}}{I_t A_{PVT}} < 1 \tag{3.11}$$

The thermal efficiency of a PVT system is generally higher than its electrical efficiency. According to Sevela and Olesen [35], it can reach a maximum of 42%.

3.6. Thermal Energy Storages (TES)

The accumulation of energy is paramount for several applications, many industrial and domestic processes require a continuous energy input. The energy supply can be intermittent during the day or the year due to impractical production or to its high cost. Therefore, a system for the storage of energy enables an efficient use of it, storing energy when is abundant or cheap and releasing it when is scarce or costly, makes the process independent of the energy supply.

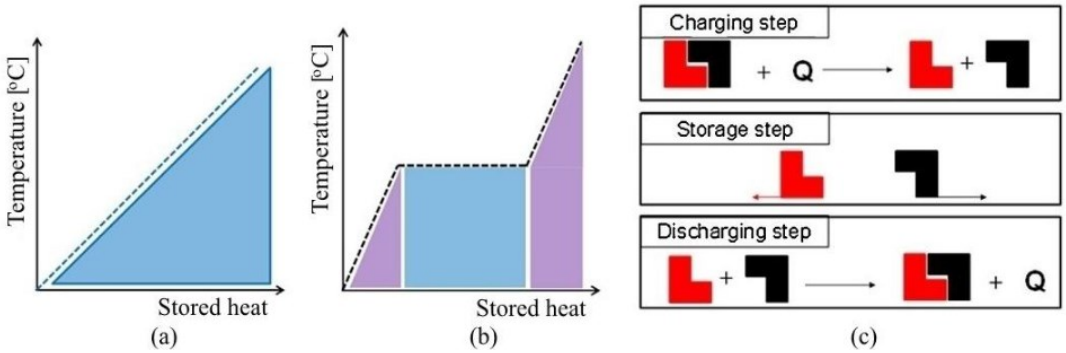

Figure 10: Different types of TES: sensible heat TES (**a**), latent heat TES (**b**), thermo-chemical TES (**c**).

Energy can be stored in various forms: as electricity in battery accumulators, as a compressed fluid in a mechanical energy storage, as a heavy lifted object in a gravitational

energy storage or as heat in a thermal energy storage (TES). In this last case, heat can be stored inside a storage medium as sensible heat, latent heat, or thermo-chemical heat (see Figure 10 [36]).

A sensible heat TES stores heat by increasing the temperature of the medium; the amount of heat stored by a mass m of the medium whose temperature increases from T_1 to T_2 is given by Equation 3.12:

$$Q = m\Delta h(T_1 \rightarrow T_2) = m\int_{T_1}^{T_2} c_p dT \tag{3.12}$$

Where c_p is the specific heat capacity of the medium. The most used medium in sensible heat TES is water, which can store a high amount of heat with a small change in temperature, due to its high specific heat. Many other materials can be used as medium, both organic liquids and solids e.g., rock, sand, cast iron, etc.

A latent heat TES stores heat by changing the phase of the medium, possibly increasing its temperature too. The amount of heat stored by a mass m of a medium whose temperature increases from T_1 to T_2, changing from phase α to phase β at the temperature T_{pc} is given by Equation 3.13:

$$\begin{aligned} Q &= m\left[\Delta h^{\alpha}(T_1 \rightarrow T_{pc}) + f\Delta h^{\alpha\rightarrow\beta}(T_{pc}) + \Delta h^{\beta}(T_{pc} \rightarrow T_2)\right] \\ &= m\int_{T_1}^{T_{pc}} c_p^{\alpha} dT + f\Delta h^{\alpha\rightarrow\beta}(T_{pc}) + m\int_{T_{pc}}^{T_2} c_p^{\beta} dT \end{aligned} \tag{3.13}$$

Where c_p^{α} and c_p^{β} are the specific heat capacities of phases α and β respectively, f is the fraction of medium that has changed phase and $\Delta h^{\alpha\rightarrow\beta}(T_{pc})$ is the latent heat associated to the phase change $\alpha \rightarrow \beta$ at the temperature T_{pc}. The media used in latent heat TES are called phase-change materials (PCM), the phase change is usually the transition between solid and liquid phase, i.e., melting. PCMs can be classified into organic, inorganic, and eutectic materials, each one with advantages and disadvantages.

In conclusion, a thermo-chemical TES stores heat by causing an endothermic chemical reaction within the medium. The amount of heat stored by a mass m of a medium involved in an endothermic chemical reaction is given by Equation 3.14:

$$Q = m\Delta h_R \tag{3.14}$$

Where Δh_R is the heat of reaction. The media used in thermo-chemical TES are called thermo-chemical materials (TCM), usually the chemical reaction involved is the decomposition of the reactants [37].

3.7. Borehole Thermal Energy Storage (BTES)

A borehole thermal energy storage system (BTES) is a specific type of sensible heat TES, which stores thermal energy in the ground [38]. It represents a very promising and inexpensive technology for heating and cooling requirements. Furthermore, it is often coupled with a heat pump system in regions where there is the necessity for a long-term thermal energy storage. It consists of a well drilled into the ground usually not deeper than 250 m, in which a working fluid, typically water, circulates in an open or closed loop inside a pipe network fixed by filling the borehole with grout material. The pipe network can have different designs, either with coaxial pipes or with U-shaped pipes (see Figure 11 [39]), it constitutes the borehole heat exchanger (BHE).

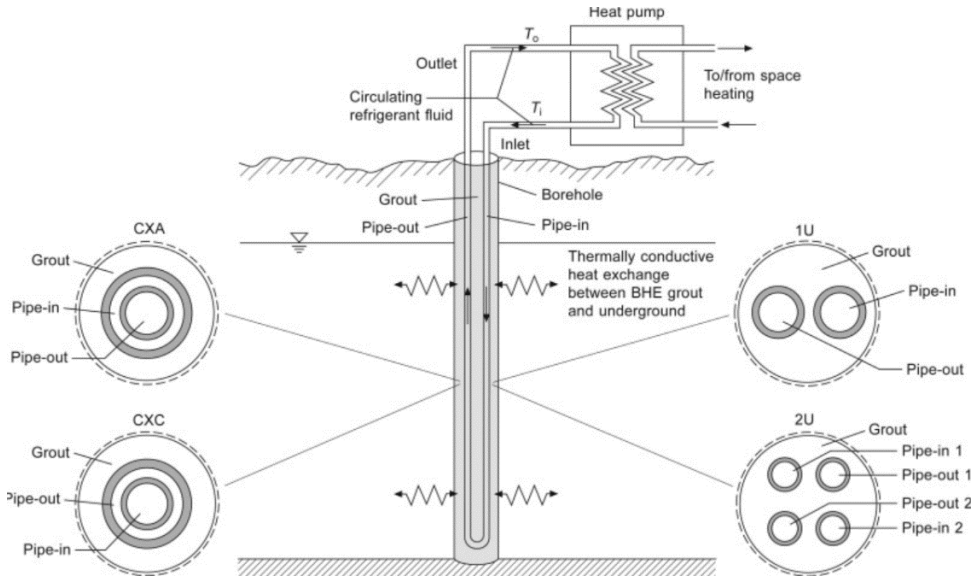

Figure 11: Scheme of a borehole TES with different pipe network designs.

Heat can be stored or extracted from the ground through the BHE, the heat transport mechanism in the ground is conduction/convection, thus it is regulated by the specific heat capacity and the thermal conductivity of the ground, whose values strongly depend on the type of soil and on the presence of underground moisture. Different soils can have very different specific heat capacity and thermal conductivity, the typical range are 0.7−1 kJ/(kg·K), and 1−5 W/(m·K) respectively [40].

4. Simulation Approach

4.1. General

A model describing the integrated energy system is built using Matlab. The zeotropic cascade heat pump is the core of the plant; therefore, it is the section modelled with the highest degree of detail. For each part of the plant some simplifying assumptions are made. They are presented and explained in the following specific sections of the document. Most of the principles for the simulation approach are taken from previous works on the topic, specifically the master's theses made by Ryssdal [6] and Skoglund [7].

The city of Oslo is the base location for building the system, meteorologic data (air temperature and solar irradiation) on hourly base were retrieved using Meteonorm [41] for year 2005. The choice of 2005 as reference year maintains the consistency with previous works [6] [7]. For the detailed simulation of the heat pump, the thermodynamic properties of the fluids are calculated using Refprop v9.1, coupled with Matlab. Refprop is a software developed by NIST (National Institute of Standards and Technology) for the evaluation of pure component and mixture thermodynamic and transport phenomena properties based on the most accurate models currently existing [42]. It is assumed that the compressors are the only unit operation of the plant that require electrical energy to work. In most industrial plants in fact, the power consumption of pumps, control systems, and other electrically-driven devices is negligible when compared to the compressor duty [43].

The heat demand for district heating is divided into water heating and space heating demands. A base demand of 50 kW for water heating, independent of outside air temperature, is assumed; while, a temperature dependency exists for the space heating demand: it increases of 10.25 kW for every Celsius degree below 15°C. The mathematical relationship defining the heat demand is reported in Equation 4.1.

$$D = \begin{cases} 50\ kW & if\ T_a \geq 15°C \\ [50 + 10.25(15 - T_a)]\ kW & if\ T_a < 15°C \end{cases} \quad (4.1)$$

Where T_a is the ambient air temperature. The trend of the heat demand in Oslo during year 2005 is shown in Figure 12.

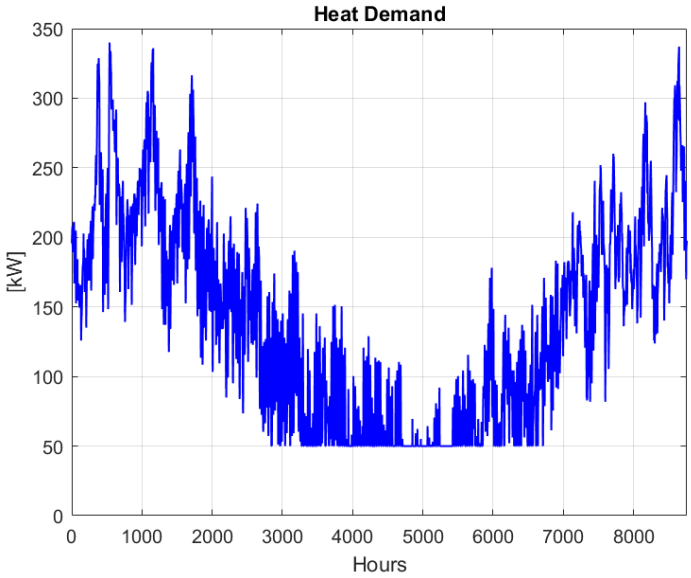

Figure 12: Heat demand for district heating throughout the year 2005 in Oslo.

4.2. Zeotropic Cascade High Temperature Heat Pump

4.2.1. Configuration

The zeotropic cascade high temperature heat pump consists of a low stage and a high stage, both comprise an evaporator, a condenser, two equal parallel compressors and an expansion valve. The two stages are nested together by means of a cascade heat exchanger, which serves as condenser for the low stage and as evaporator for the high stage. For both stages an internal heat exchanger (IHX) can be present. It permits to integrate the vapor superheating at the evaporator outlet with the liquid subcooling at the condenser outlet. Once the temperature levels in those points are known, it will be possible to determine if the IHXs are applicable; superheater and subcooler with external utilities are used otherwise. A configuration with two parallel compressors for both stages is useful for load and capacity control, one of the compressors can be shut-off when the heat demand is low, increasing the plant's energy efficiency. A PFD of the heat pump section obtained after sizing is shown in Figure 13.

The following assumptions are made for modelling the heat pump:

- In the cascade heat exchanger, the low stage and the high stage refrigerants exchange the same heat capacity.
- Saturated vapor is present at the outlet of the evaporators.
- Saturated liquid is present at the outlet of the condensers.

- The expansion process is isenthalpic.
- The pressure drops and the heat losses in the system are neglected.
- All the heat exchangers have a counter-flow configuration.

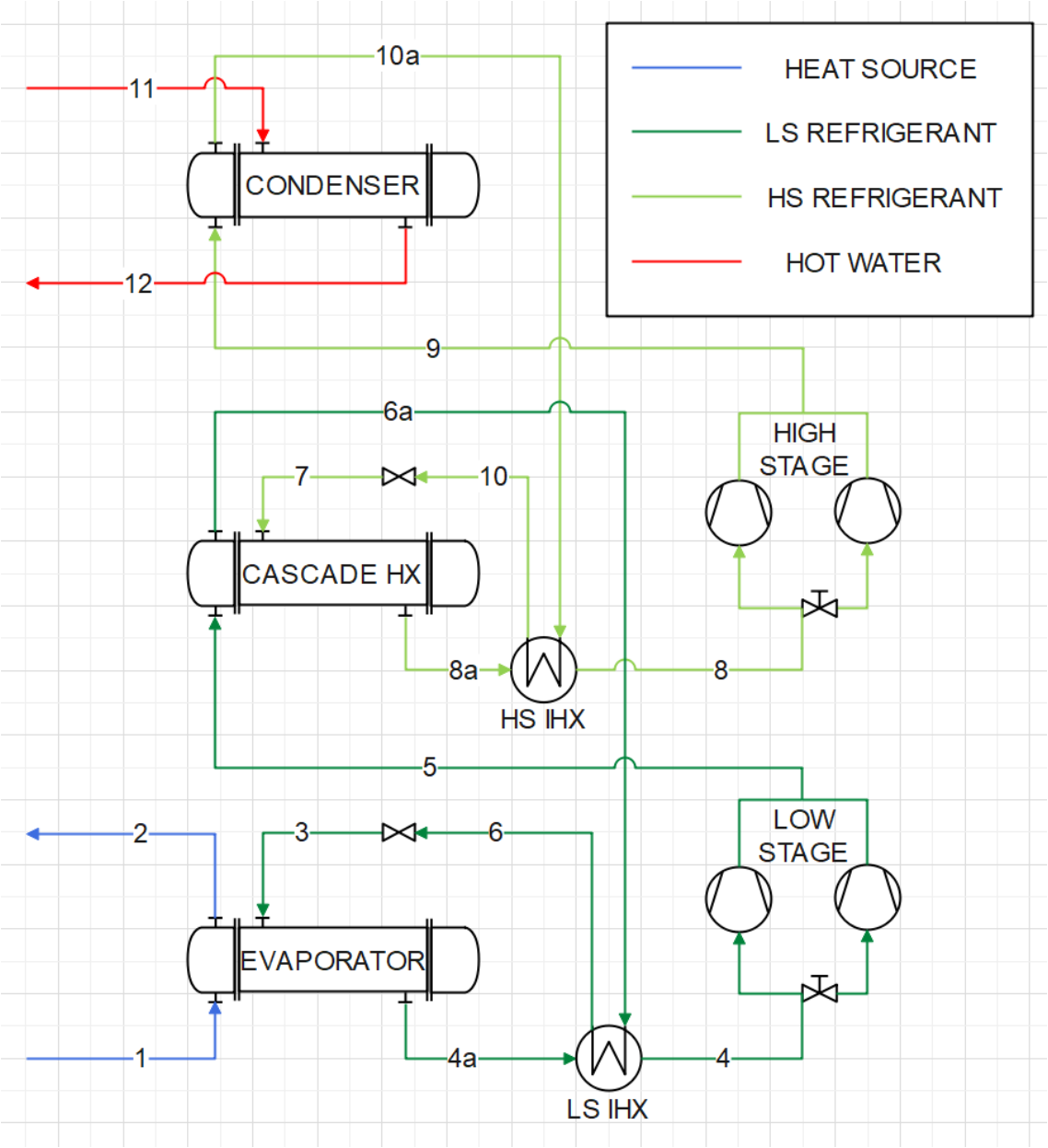

Figure 13: PFD of the heat pump section.

4.2.2. Refrigerant Selection

A two-stage cascade heat pump requires the selection of two refrigerants such that the critical point of the one used in the high stage has a higher critical point than the one used in the low stage. Natural working fluids such as ammonia, carbon dioxide, light alkanes

and alkenes, thanks to their negligible ODP, have a lower impact on the environment compared to synthetic refrigerants (HFCs and CFCs). Therefore, natural working fluids must be the primary choice as refrigerants. Sarkar and Bhattacharyya made a comparison in terms of performance between pure hydrocarbons and CO_2/hydrocarbon blends utilized as refrigerants in a heat pump [44]. Results showed that, due to gliding temperature during evaporation and condensation, the zeotropic blends (specifically CO_2/butane and CO_2/isobutane) can be employed very effectively in heat pumps, instead of their pure counterparts. Ganesan and Eikevik showed that CO_2/butane and CO_2/pentane zeotropic mixtures with higher content of CO_2 result in higher power consumption of the compressor and lower COP of the heat pump [8]. This generally happens if the heat source temperature is above 20°C (see Figure 14). Zeotropic mixtures with a small content of CO_2 (lower than 10%) should be selected.

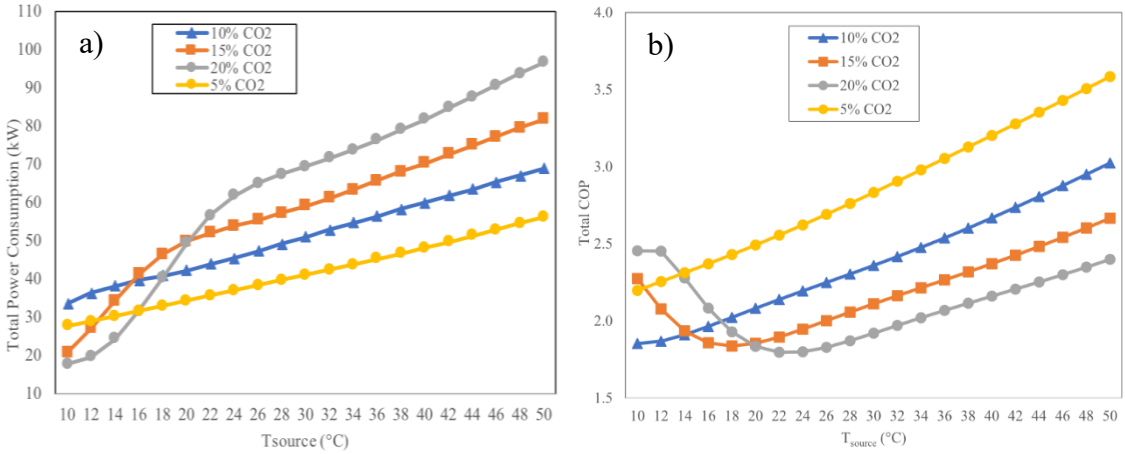

Figure 14: Impact of the source temperature on power consumption (**a**) and COP (**b**) of the HP, at various CO2 contents.

As suggested by Skoglund, the key approach to select the refrigerant mixtures is to minimize the pressure levels and at the same time having a good temperature profile match in the main heat exchangers between the contacted fluids [7]. In his thesis work, Skoglund used pure propane and 5/95% CO_2/butane mixture as low stage and high stage refrigerants respectively. He reported that the condensation pressure levels obtained in the cascade heat pump were 2,440 kPa and 1,800 kPa. From the cost estimation point of view, the capital investment of a operation unit increases significantly if the pressure inside is higher than 10-12 bar, because thicker walls or special materials are needed [43] [45]. Therefore, a reasonable assumption is to set the condensation pressures lower than 12 bar.

CO_2/butane and CO_2/pentane blends are selected for low stage and high stage respectively, their vapor-liquid equilibria and temperature glides at different composition are shown in Figure 15.

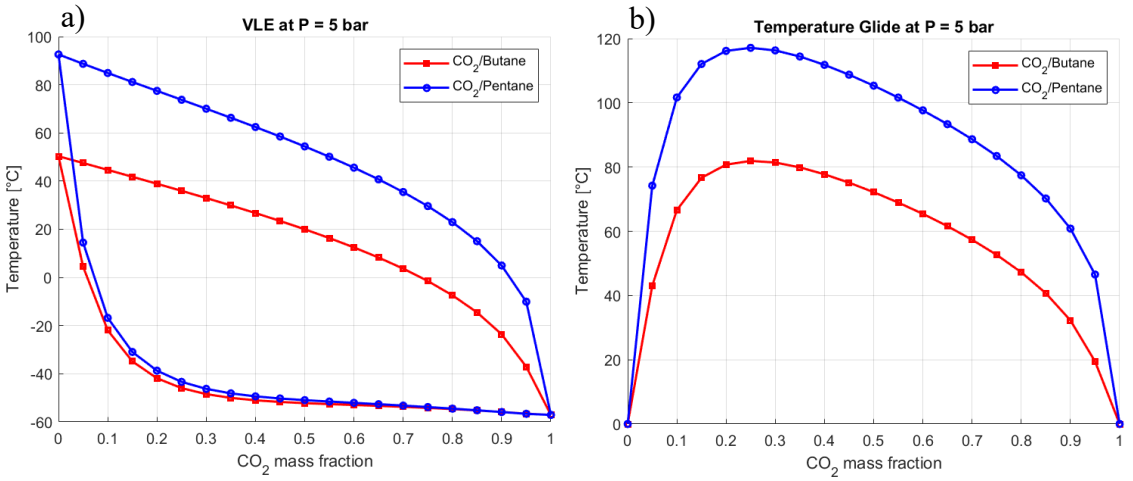

Figure 15: VLE (**a**) and temperature glide (**b**) at 5 bar for CO2/butane and CO2/pentane blends.

As it can be seen, if the CO_2 mass fraction is increased from 0 to 10%, then the bubble temperature of both blends decreases much faster than the dew temperature, which only varies from 50 to 45°C. Given the mixture pressure, its dew temperature can reasonably be assumed constant, for a CO_2 content lower than 10%.

Focusing first on the high stage refrigerant, it contacts the hot water inside the condenser; an inlet temperature of 70°C is assumed for hot water, while, for the design specification, it has to exit at least at 100°C. It is desirable to have a difference of around 5-10°C

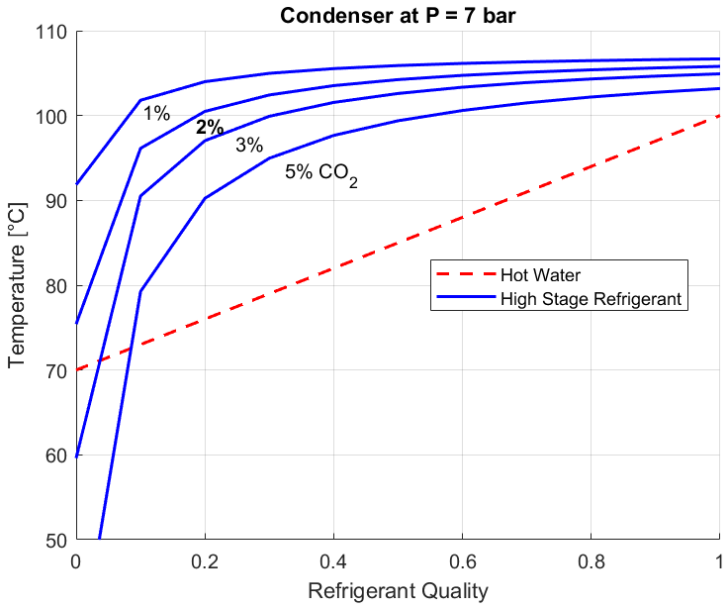

Figure 16: Temperature coupling in the condenser between hot water and CO2/pentane mixtures at different compositions.

between contacted fluids in the heat exchangers, thus the high stage condensation pressure should be around 7 bar, leading to a CO_2/pentane dew temperature between 103 and 106°C (see Figure 16). Inside the condenser the temperature profiles of the contacted fluids should be close to each other, but must not cross; therefore, as shown in Figure 16, the best mixture to select is 2/98% CO_2/pentane, ensuring the best fluid coupling.

Similarily, the refrigerant to be used in the low stage can be selected. This time it contacts the heat source in the evaporator, for which an inlet temperature of 40°C and an outlet temperature of 30°C are assumed. The evaporation pressure that ensures a temperature difference between the fluids at the evaporator outlet of 5-10°C is around 3 bar, resulting in a dew temperature of the mixture of 30°C. In this case the refrigerant enters the exchanger as a liquid/vapor mixture with roughly a 10% vapor quality, because it is expandend in the valve. For that reason, not all the latent heat of vaporization is exchanged. As it can be seen in Figure 17, the closest line to the heat source one, that does not cross it, is relative to the 1/99% CO_2/butane mixture. However, during the heat exchange, the temperature difference between the fluids gets too low (less than 3°C), the same happens for the 2/98% mixture; therefore, the refrigerant ensuring the best coupling for the low stage is the 3/97% CO_2/butane mixture.

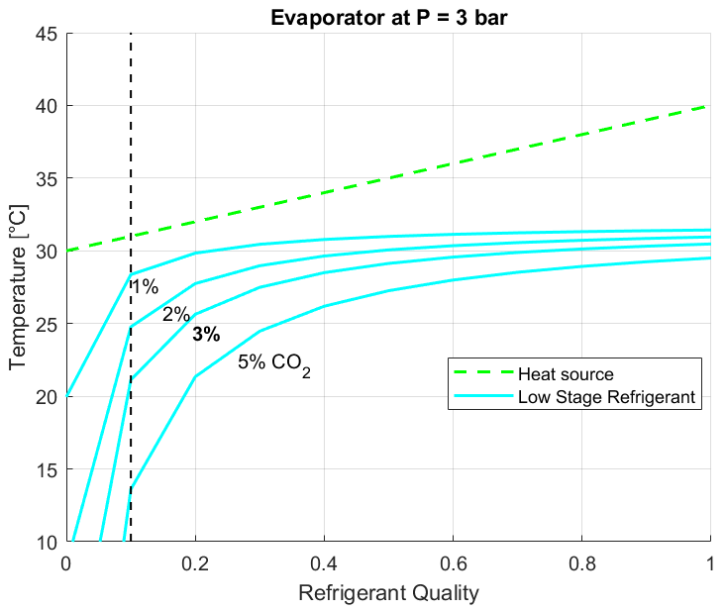

Figure 17: Temperature coupling in the evaporator between heat source and CO2/butane mixtures at different compositions.

The choice of the correct refrigerant can be verified after the heat pump is sized, by looking the actual temperature trends inside the heat exchangers.

4.2.3. Sizing

Once the two zeotropic refrigerants are selected for both stages, the cascade heat pump can be sized, based on two main design specifications: hot water temperature higher than 100°C and COP of the heat pump higher than 3.6. From the air temperature data in Oslo in year 2005, the heat demand for district heating can be calculated on an hourly basis with Equation 4.1 (see Figure 12). By sorting the heat demand in a complementary cumulative form, the load-duration curve (LDC) for the heat pump can be drawn (see Figure 18). The area below the LDC represents the total heat demand in the whole year, a heat pump delivering heat to such system should cover at least 90% of the total demand.

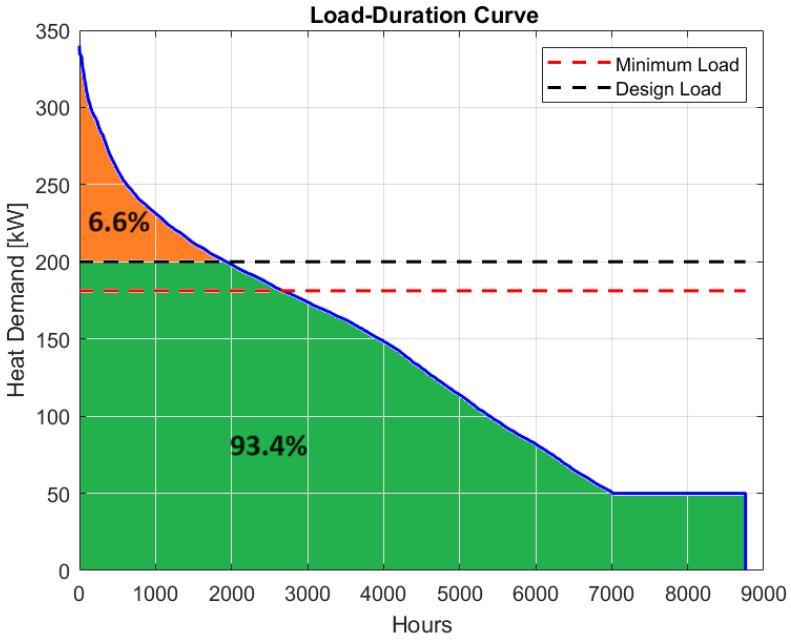

Figure 18: Load-duration curve of the heat pump, with minimum load and selected design load.

By numerically integrating the LDC, it results that the minimum capacity of a heat pump operating at maximum load is 181.2 kW. Hence, the heat pump is sized to deliver 200 kW when operating full load. This will cover 93.4% of the total heat demand, leaving the system with insufficient heating for 1950 hours during the year.

Inlet and outlet temperatures of both heat source and heat sink are decided at this level. The values of condensation pressure of both stages and evaporation pressure of the low stage are assigned such that a good temperature coupling will result, given the previously selected refrigerants. To complete the set of information required for sizing, the mass flow rates of the two refrigerants are assumed to be the same. The degrees of superheating for both stages and the temperature difference between the stages are imposed. A

superheating degree of 12°C is enough to avert refrigerant condensation inside the compressors, while a difference of 8°C between the dew point of the refrigerants in the cascade heat exchanger should ensure a good temperature profile coupling. The values assumed for the all the above-mentioned sizing parameters are reported in Table 1.

Table 1: Values assumed for the sizing parameters.

Sizing Parameter	Value
Heat source inlet temperature (T_1)	40°C
Heat source outlet temperature (T_2)	30°C
Heat sink inlet temperature (T_{11})	70°C
Heat skink outlet temperature (T_{12})	100°C
Low stage evaporation pressure (P_e^{LS})	3 bar
Low stage condensation pressure (P_c^{LS})	9 bar
High stage condensation pressure (P_c^{HS})	7.5 bar
Superheating degrees (T_{sup}^{LS}) & (T_{sup}^{HS})	12°C
Temperature difference between stages (T_{diff})	8°C

The state property values are computed in all the points of the heat pump, starting from the low stage. The compression steps are not considered to be ideal, instead they have an efficiency lower than 100%. Both isentropic and volumetric efficiencies of the compressors depend on the compression ratio of the vapor. As described in Ryssdal's work [6], a power series correlation is assumed, it is reported in Equations 4.2-4.3.

$$\eta_S = -0.00000461\, r^6 + 0.00027131\, r^5 - 0.00628605\, r^4 + 0.07370258\, r^3 - 0.46054399\, r^2 + 1.40653347\, r - 0.87811477 \quad (4.2)$$

$$\eta_V = 0.0011\, r^2 - 0.0487\, r + 0.9979 \quad (4.3)$$

Where r is the compression ratio, either of the low stage or of the high stage compressor. Once all the state properties are calculated, based on the 200 kW of condenser capacity to be obtained, the mass flow rate of the refrigerants and the capacities of cascade heat exchanger and evaporator can be calculated according to Equations 4.4-4.7.

$$\dot{m}_{ref}^{HS} = \frac{\dot{Q}_c}{h_9 - h_{10a}} \quad (4.4)$$

$$\dot{Q}_{che} = \dot{m}_{ref}^{HS}(h_{8a} - h_7) \tag{4.5}$$

$$\dot{m}_{ref}^{LS} = \frac{\dot{Q}_{che}}{h_5 - h_{6a}} \tag{4.6}$$

$$\dot{Q}_e = \dot{m}_{ref}^{LS}(h_{4a} - h_3) \tag{4.7}$$

Where the h_i is the specific enthalpy in point i (see Figure 13 for number reference). The electrical power duties of the compressors can be calculated according to Equations 4.8-4.9.

$$\dot{W}_c^{LS} = \dot{m}_{ref}^{LS}(h_5 - h_4) \tag{4.8}$$

$$\dot{W}_c^{HS} = \dot{m}_{ref}^{HS}(h_9 - h_8) \tag{4.9}$$

For the calculation of the heat exchangers' area, a value for all the global heat transfer coefficients must be assumed. For the three main heat exchangers, the same values as in Skoglund's work are taken [7], they are reported in Table 2.

Table 2: Values assumed for the global heat transfer coefficients.

Heat exchanger	**Global heat transfer coefficient [W/(m²K)]**
Condenser	1400
Cascade Heat Exchanger	1800
Evaporator	1600
Internal Heat Exchangers	1000

From the capacities of the heat exchangers and the temperature levels of the fluid inside them, the areas can be calculated according to Equation 4.10.

$$A_{HX} = \frac{\dot{Q}_{HX}}{U_{HX}\Delta T_{ml}^{HX}} \tag{4.10}$$

Where U_{HX} represents the global heat transfer coefficient of a generic heat exchanger and ΔT_{ml}^{HX} is the logarithmic mean temperature difference of the fluids, whose definition is given in Equation 4.11.

$$\Delta T_{ml}^{HX} = \frac{\theta_{HX}^{in} - \theta_{HX}^{out}}{\ln\left(\frac{\theta_{HX}^{in}}{\theta_{HX}^{out}}\right)} \tag{4.11}$$

Where θ_{HX}^{in} and θ_{HX}^{out} represent the temperature difference between the contacted fluids at the inlet and outlet of a generic heat exchanger.

The areas of all the heat exchangers of the heat pump resulting from the sizing procedure are listed in Table 3, together with their scaling to commercial values.

Table 3: Exchanger area of all the heat exchangers resulting from sizing, with the scaling to commercial values.

Heat Exchanger	Exchange Area [m^2]
Condenser	12.69 → 13
Cascade HX	12.76 → 13
Evaporator	13.83 → 14
Low stage IHX	1.16 → 1.2
High stage IHX	3.70 → 3.7

The last information that derives from the sizing procedure is the size of the compressors. The formula used for the calculation considers the volumetric efficiency η_V, it is reported in Equation 4.12.

$$V_c = 3{,}600\ \frac{\dot{m}_{ref}}{\eta_V \rho_{in}} \tag{4.12}$$

Where $\dot{m}_{ref}$ is the mass flow rate of the vapor refrigerant to be compressed, ρ_{in} is its mass density and the factor 3,600 is for the conversion between seconds and hours. The flow of refrigerant is split between two equal parallel compressors; therefore, the size of a single compressor is half of the one deriving from Equation 4.12. The values are reported in Table 4 and scaled to the commercial values.

Table 4: Compressor sizes resulting from sizing, with the scaling to commercial values.

Compressor	Size [m^3/h]
Low Stage	158.72 → 160
High Stage	164.13 → 165

The mass flow rates of both heat source and heat sink can be used as inputs for the heat pump, their values are given by Equation 4.13-4.14.

$$\dot{m}_{hs} = \frac{\dot{Q}_e}{c_p(T_1 - T_2)} \tag{4.13}$$

$$\dot{m}_{hw} = \frac{\dot{Q}_c}{c_p(T_{12} - T_{11})} \tag{4.14}$$

The heat source mass flow rate results to be 4.11 kg/s, while the heat sink mass flow rate results to be 1.59 kg/s. Finally the COP of the heat pump can be estimated according to Equation 4.15.

$$COP = \frac{\dot{Q}_c}{\dot{W}_c^{LS} + \dot{W}_c^{HS}} \tag{4.15}$$

The resulting COP of the heat pump is around 3.15, which is lower than the threshold imposed by the design specification. The energy efficiency of the system, thus the COP, can be increased by applying an energy integration procedure (see Chapter 4.2.5). Two streams of the heat pump, one to be heated the other one to be cooled, can be contacted if their temperature allow heat exchange. In this way the use of external utilities, such as steam or cooling water, can be reduced or eliminated, reducing at the same time the operational costs.

4.2.4. Operational Modes

The design of the heat pump is based on the heating capacity that it must deliver for district heating, namely 90% of the total annual demand when the heat pump operates on full load. When the demand of energy is low, it is not necessary to operate the heat pump at full load mode, a part load mode is selected instead. When the heat pump operates on part load, it produces a fraction of the full load capacity, at the same time consuming a fraction of the full load compression duty. The heat pump can operate on part load also when the available power is insufficient for the full load mode.

The sizing procedure presented in Section 4.2.3, assumed that the heat pump operated on part load mode produces half the capacity of when it operates on full load. In that case, a simple way to switch between full load and part load is to shut-off one of the parallel compressors, which halves the mass flow rate of refrigerant, the power consumption, and the condenser capacity. To maintain constant temperature levels between the two operational modes in the heat exchangers, the exchange areas of all the heat exchangers must be halved. This in practice can be obtained by physically closing to the refrigerants flow part of the exchangers.

4.2.5. Energy Integration

For the designed heat pump a simple energy integration within the system is applicable. It is useful to improve the energy efficiency, and to meet the specification imposed on the COP. According to the sizing procedure applied, the high stage IHX cannot completely subcool the refrigerant exiting the condenser from 80°C to 54°C, because the heat transfer is not permitted with the same refrigerant to be superheated from 65°C to 77°C. An external utility would be necessary to perform the subcooling. An energy integration solution that avoids the use of other utilities and at the same time increases the COP, is to split the subcooling in two steps. The first part of the subcooling can be performed in the condenser, assuming the hot water entering at 60°C and lowering the refrigerant temperature to 65°C. With 5°C of difference the temperature coupling is maintained good. The remaining part of the subcooling, from 65°C to 54°C can be conducted with a process

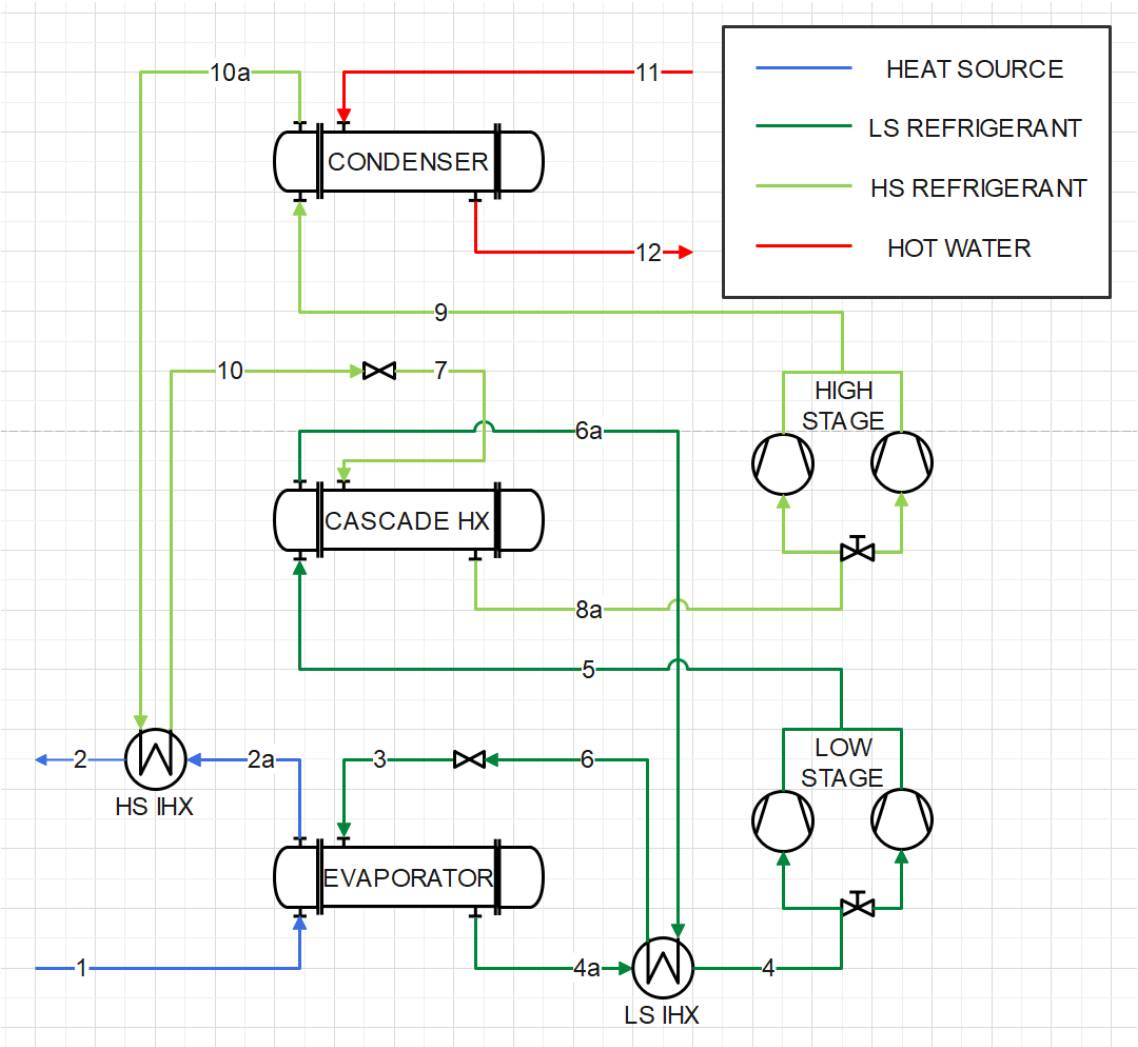

Figure 19: PFD of the heat pump section after energy integration.

stream at least 10°C colder, that needs to be heated. An example is the heat source leaving the evaporator, which must be re-heated from 30°C to 40°C, hence the IHX is not eliminated but simply moved. The superheating of the high stage refrigerant now remains undetermined. A simple solution, that would in turn increase the COP, is to carry out the superheating inside the cascade heat exchanger, thus contacting the two refrigerants. The heat pump scheme after energy integration is shown in Figure 19.

After energy integration the values of the design parameters have changed. The new values, for both full load and part load, are listed in Table 5.

Table 5: Values of the design parameters of the heat pump after energy integration, for full load and part load.

Design Parameter	Full Load	Part Load
Condenser Area [m^2]	18.57 → 22	9.28 → 11
Cascade HX Area [m^2]	11.65 → 12	5.82 → 6
Evaporator Area [m^2]	12.63 → 13	6.32 → 6.5
Low Stage IHX Area [m^2]	1.06 → 1.1	0.53 → 0.55
High Stage IHX Area [m^2]	0.48 → 0.5	0.24 → 0.25
LS Compressor Size [m^3/h]	289.88 → 290	144.94 → 145
HS Compressor Size [m^3/h]	296.96 → 300	148.48 → 150

The new flow parameters of heat source and heat sink streams are listed in Table 6.

Table 6: Values of the inlet flow parameter of heat source and heat sink for full load and part load.

Stream	Flow Parameter	Full Load	Part Load
Heat Source	Inlet Temperature	40°C	40°C
	Mass Flow Rate	3.76 kg/s	1.88 kg/s
Heat Sink	Inlet Temperature	60°C	60°C
	Mass Flow Rate	1.19 kg/s	0.60 kg/s

After energy integration the value of the COP estimated with sizing is 3.51, it is still lower than 3.6, but now it can easily meet the design specification by slightly increasing the condenser area, which means increasing the heat capacity of the heat pump. Choosing a condenser area of 22 m^2, rather than 19 m^2, will allow the COP to overcome the threshold of 3.6.

4.2.6. Algorithm

The zeotropic cascade high temperature heat pump, that has been sized with energy integration, can then be simulated. Given the input conditions (mass flow rate and inlet temperature of both heat source and heat sink), all the output variables (condenser capacity, compressor work, COP, and hot water outlet temperature) of the heat pump system are calculated with an iterative procedure.

Each iteration starts with an estimate of the low stage evaporation temperature T_e^{LS}, the low stage condensation temperature T_c^{LS} and the high stage condensation temperature T_c^{HS}. Note that, since the refrigerants are zeotropic mixtures, evaporation and condensation temperatures are not unique; the evaporation temperature is taken equal to the mixture's dew point, while the condensation temperature is taken equal to the mixture's bubble point. All the state properties of the heat pump are calculated, with specified superheating degree and temperature difference between the stages. Then the capacities of all the main heat exchangers can be computed. Every heat exchanger is characterized by a logarithmic mean temperature difference (LMTD), which has two mathematical expressions: one is the actual logarithmic mean of the temperature differences between inlet and outlet, the other comes from the global energy balance of the heat exchanger. The three equations based on the exchanger LMTDs are reported in Equations 4.16-4.18.

$$\Delta T_{ml}^{c} = \frac{\dot{Q}_c}{U_c A_c} = \frac{(T_9 - T_{12}) - (\boldsymbol{T_c^{HS}} - T_{11})}{\ln\left(\frac{T_9 - T_{12}}{\boldsymbol{T_c^{HS}} - T_{11}}\right)} \tag{4.16}$$

$$\Delta T_{ml}^{che} = \frac{\dot{Q}_{che}}{U_{che} A_{che}} = \frac{(T_5 - T_{8a}) - (\boldsymbol{T_c^{LS}} - T_7)}{\ln\left(\frac{T_5 - T_{8a}}{\boldsymbol{T_c^{LS}} - T_7}\right)} \tag{4.17}$$

$$\Delta T_{ml}^{e} = \frac{\dot{Q}_e}{U_e A_e} = \frac{(T_1 - \boldsymbol{T_e^{LS}}) - (T_2 - T_3)}{\ln\left(\frac{T_1 - \boldsymbol{T_e^{LS}}}{T_2 - T_3}\right)} \tag{4.18}$$

The system of algebraic equations composed by Equations 4.16-4.18 cannot be solved through an analytical method but require a numerical solution. The Matlab solver fsolve, specifically made for the numerical solution of systems of non-linear equations is used. Fsolve solves the function minimization problem shown in Equation 4.19.

$$\min_{T_e^{LS},T_c^{LS},T_c^{HS}} \{|E_c(T_e^{LS},T_c^{LS},T_c^{HS})|, |E_{che}(T_e^{LS},T_c^{LS},T_c^{HS})|, |E_e(T_e^{LS},T_c^{LS},T_c^{HS})|\} \quad (4.19)$$

Where the function E_i are the errors specific for each heat exchanger, defined as the difference between the two definitions of LMTD (Equations 4.16-4.18). The iterative procedure is therefore carried out inside fsolve, without the need of building a while cycle in the code. It returns the approximated values of T_e^{LS}, T_c^{LS} and T_c^{HS} such that the errors E_c, E_{che} and E_e are below the default tolerance of fsolve i.e., 10^{-6}. This approach for solving the zeotropic heat pump system is more suitable than the one proposed by Ryssdal [6] and used by Skoglund [7] in their works, because it accounts for the variation of temperature during evaporation and condensation of the refrigerants.

4.2.7. Heat Pump Results

The simulation of the heat pump using the algorithm described in Section 4.2.6, allows the calculation of all the outlet parameters of the heat pump, both for the full load and the part load operations. They are reported in Table 7. An energy efficiency of 85% is assumed for the compressors.

Table 7: Results of the heat pump operation for both full load and part load operations.

Parameter	Full Load Value	Part Load Value
Heat Pump Heat Capacity	200.6 kW	100.4 kW
Heat Pump Power Consumption	55.8 kW (65.6 kW)	27.8 kW (32.7 kW)
Hot Water Outlet Temperature	**100.3°C**	**100.4°C**
Coefficient of Performance (COP)	**3.60**	**3.61**

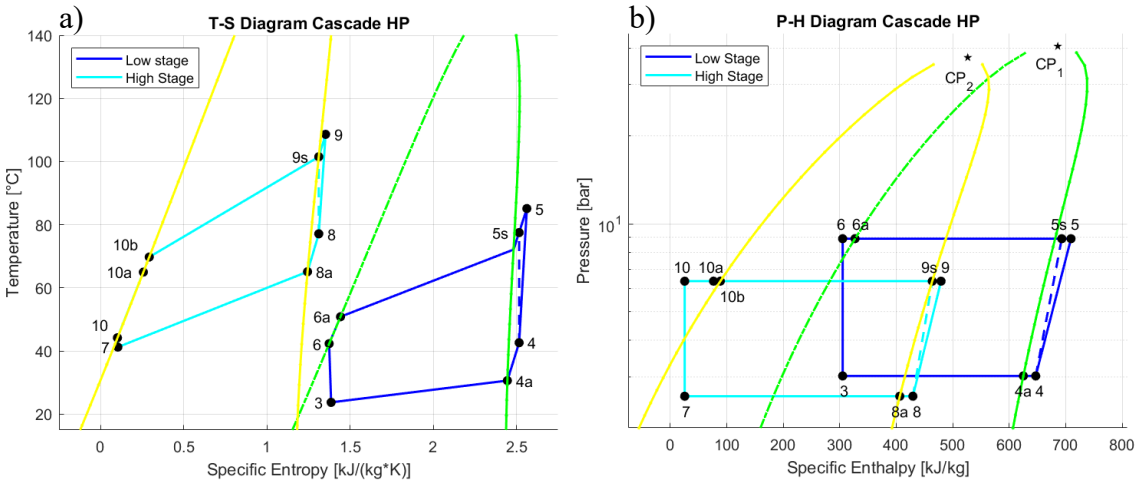

Figure 20: T-s (**a**) and P-h (**b**) diagrams representing the heat pump.

Once calculated the exact values of the state properties in every point of the system, the two cascaded cycles can be easily visualized in the T-s and P-h diagrams shown in Figure 20.

Since the type of the heat exchangers have not been decided, it is assumed that the heat flux between contacted fluids is uniform and independent of the phase changes. The heat exchangers are divided in slices. A fraction of the total heat flow is transferred inside each slice, allowing to track the temperature profiles of the fluids and in turn the LMTDs values. All the profiles inside the three main heat exchangers (evaporator, cascade heat exchanger and condenser) are shown in Figure 21.

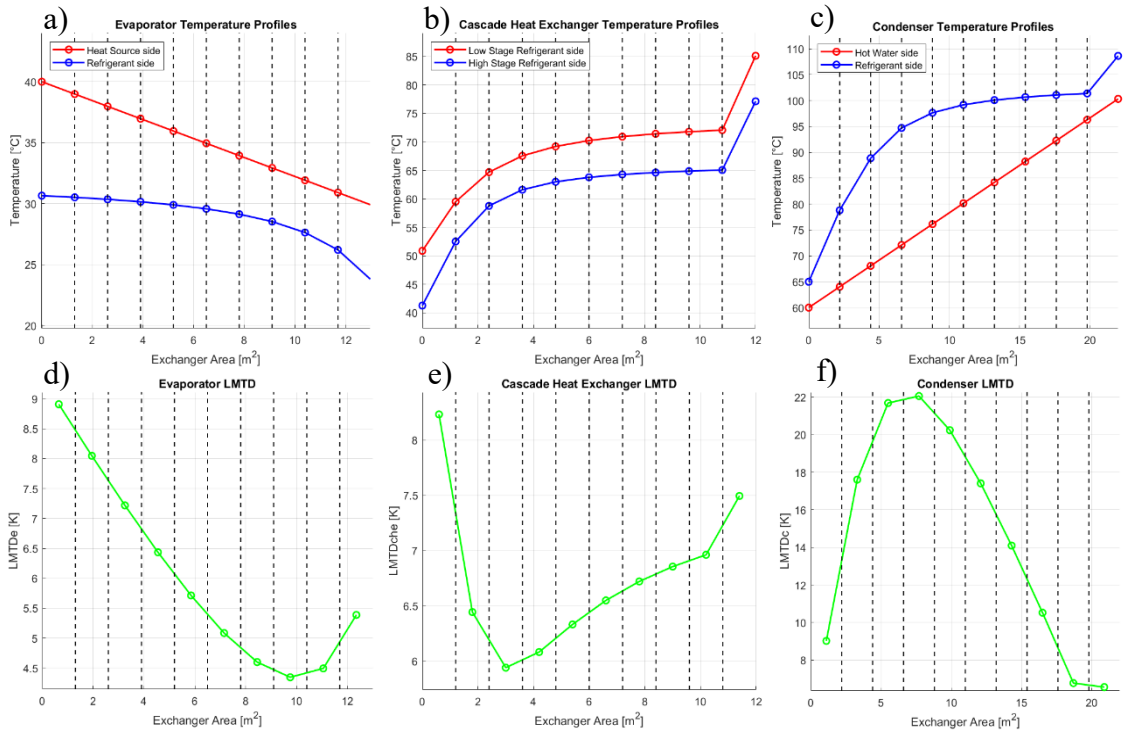

Figure 21: Temperature profiles (**a, b, c**) and LMTDs (**d, e, f**) inside the three main heat exchangers.

From Figure 21, it is clear that the refrigerants selected ensure a good temperature profile coupling, so that the internal LMTDs are never below 4°C. Inside the condenser the LMTD between high stage refrigerant and hot water reaches 22°C; this value is very high, and it is not possible to decrease it, due to the shape of the gliding temperature of the CO_2/pentane mixture (see Figure 16). However, once the type of heat exchanger is assumed, information about the fluid dynamics and the heat transfer inside can be deducted, enabling a more detailed description of the internals.

4.3. Photovoltaic/Thermal (PVT) Model

4.3.1. Configuration

Photovoltaic/thermal (PVT) panels are used to collect solar energy from the sun and convert it into electrical and thermal energy, useful to drive the compressors and re-heat the heat source of the heat pump. The photovoltaic/thermal panels are described using a very simple model: the solar incident radiation that hits the solar collector is converted into both electrical energy and thermal energy with certain electrical and thermal efficiencies. With the solar irradiance data collected with Meteonorm, specific for Oslo in the year 2005, the electrical and thermal generation data on an hourly base can be obtained. Thermal and electrical efficiencies are not considered to be constant. Instead they vary depending on the system conditions, and they are calculated according to the methods presented in the work of Herrando et al. [46].

Starting with the thermal efficiency of the PVT collector, there is not a standard approach for the assessment its performance. ISO and ASHRAE are two methods based on steady-state testing of the PVT panels. In this thesis, the ISO method is preferred. It models the PVT thermal efficiency according to Equation 4.20.

$$\eta_{th} = \eta_O - a_1 T_r - a_2 I_t {T_r}^2 \tag{4.20}$$

Where η_O is the optical efficiency, a_1 is the linear heat loss coefficient, a_2 is the quadratic heat loss coefficient, I_t is the total solar irradiance per unit of area and T_r is the reduced temperature, whose definition is given by Equation 4.21.

$$T_r = \frac{\overline{T_f} - T_a}{I_t} \tag{4.21}$$

In which $\overline{T_f}$ is the average cooling fluid temperature, namely the arithmetic mean between inlet and outlet heat source temperatures and T_a is the air temperature. When the total solar irradiance I_t is zero or close to zero, then mathematically the thermal efficiency would tend to minus infinity; to avoid this possibility, the thermal efficiency is set to zero when the sun is low.

For what concerns the electrical efficiency, it strongly depends on the PV cell temperature according to Equation 4.22.

$$\eta_{th} = \eta_{ref}\left[1 - \beta_0\left(T_{PV} - T_{ref}\right)\right] \tag{4.22}$$

Where η_{ref} is the reference PV module efficiency tested at the reference temperature T_{ref} of 25°C and at a solar irradiance of 1000 W/m^2, β_0 is the temperature coefficient of the PV module, while T_{PV} is the surface temperature of the PV module, which is assumed to be 20°C higher than the air temperature.

The PVT panel type will not be specified, the values of all the coefficients defining the PVT module efficiencies are taken from previous works [6] [7], listed in Table 8.

Table 8: PVT module features.

PVT Features	Value
Optical Efficiency η_O	0.51
Linear Heat Loss Coefficient a_1	4.93 W/(m^{2}K)
Quadratic Heat Loss Coefficient a_2	0.021 W/(m^{2}K^2)
Reference Electrical Efficiency η_{ref}	0.147
Temperature Coefficient β_0	-0.0045 K^{-1}
Reference Temperature T_{ref}	25°C
Total Panels Area A_{PVT}	4000 m^2

4.3.2. Algorithm

At the kth time iteration, the air temperature and solar irradiance data ($T_a^{(k)}$ and $I_t^{(k)}$) are the inputs to the PVT model. The model calculates the electrical and thermal efficiencies ($\eta_{el}^{(k)}$ and $\eta_{th}^{(k)}$) using Equations 4.20-4.22, if the thermal efficiency results to be negative, it is set to zero. Eventually, knowing the total area of the PVT panels, the model calculates the electrical and thermal power generated according to Equations 4.23-4.24.

$$\dot{P}_{el}^{(k)} = \eta_{el}^{(k)} I_t^{(k)} A_{PVT} \tag{4.23}$$

$$\dot{P}_{th}^{(k)} = \eta_{th}^{(k)} I_t^{(k)} A_{PVT} \tag{4.24}$$

4.4. Battery Model

4.4.1. Configuration

The energy that can be obtained from the sun with a solar collector is discontinuous during the day, due to day/night switch, variable cloud coverage, and other atmospheric factors.

It is also variable throughout the year, because of the difference in daytime duration between summer and winter. A battery is an energy accumulator that can store a certain amount of electrical energy and release it when needed. In this thesis work it is simulated according to a greatly simplified model. A battery type will not be specified and, for sake of simplicity, the maximum capacity and the charging/discharging efficiency will be the only two parameters characterizing the battery accumulator. Their values are reported in Table 9.

Table 9: Battery features.

Battery Features	Value
Maximum Capacity B_{max}	1000 kWh
Round-trip Efficiency η_B	80% [6]

4.4.2. Algorithm

Initially the energy stored in the battery accumulator is set to be 75% of the total capacity B_{max}. At every time iteration, the battery either charges or discharges depending on the heat pump demand and on the PVT supply ($\dot{W}_c^{(k)}$ and $\dot{P}_{el}^{(k)}$). During charging, the amount of electrical energy stored at the k[th] iteration is given by Equation 4.25.

$$\begin{aligned} B^{(k)} &= B^{(k-1)} + \eta_B \int_{t_{k-1}}^{t_k} \left(\dot{P}_{el} - \dot{W}_c\right) dt \\ &= B^{(k-1)} + \eta_B \left(\dot{P}_{el}^{(k)} - \dot{W}_c^{(k)}\right) \cdot 1h \end{aligned} \tag{4.25}$$

During discharging Equation 4.26 is used instead.

$$\begin{aligned} B^{(k)} &= B^{(k-1)} - (2 - \eta_B) \int_{t_{k-1}}^{t_k} \left(\dot{W}_c - \dot{P}_{el}\right) dt \\ &= B^{(k-1)} - (2 - \eta_B) \left(\dot{W}_c^{(k)} - \dot{P}_{el}^{(k)}\right) \cdot 1h \end{aligned} \tag{4.26}$$

4.5. Borehole Thermal Energy Storage (BTES) Model

4.5.1. Configuration

A borehole thermal energy storage (BTES) is integrated in the system to store the thermal energy produced by the PVT panels. The thermal energy obtained from the PVT collector is subjected to significant variations, it is necessary to collect it in a storage system. The

BTES is not designed in detail, the number and the features of the pipes in the borehole heat exchanger (BHE) have not been decided and the heat transfer within the BHE is not investigated. Furthermore, a strong assumption is made on the BTES: the heat stored in it never gets below 1% of the maximum capacity, because a small amount of heat can be extracted from the ground. The BTES will be characterized only by its total storage capacity and by a loading/unloading efficiency. Their values are reported in Table 10.

Table 10: BTES features.

BTES Features	Value
Maximum Capacity H_{max}	100,000 kWh
Loading/Unloading Efficiency η_H	90% [7]

4.5.2. Algorithm

The simulation of the BTES system is based on the same simplified model as the battery accumulator. Initially the energy stored in the BTES is set to be 75% of the total capacity H_{max}. At every time iteration, the BTES is either loaded or unloaded depending on the heat pump demand and on the PVT supply ($\dot{Q}_e^{(k)}$ and $\dot{P}_{th}^{(k)}$). During loading, the amount of thermal energy stored at the k[th] iteration is given by Equation 4.27.

$$\begin{aligned} H^{(k)} &= H^{(k-1)} + \eta_H \int_{t_{k-1}}^{t_k} \left(\dot{P}_{th} - \dot{Q}_e\right) dt \\ &= H^{(k-1)} + \eta_H \left(\dot{P}_{th}^{(k)} - \dot{Q}_e^{(k)}\right) \cdot 1h \end{aligned} \tag{4.27}$$

During unloading Equation 4.28 is used instead.

$$\begin{aligned} H^{(k)} &= H^{(k-1)} - (2 - \eta_H) \int_{t_{k-1}}^{t_k} \left(\dot{Q}_e - \dot{P}_{th}\right) dt \\ &= H^{(k-1)} - (2 - \eta_H) \left(\dot{Q}_e^{(k)} - \dot{P}_{th}^{(k)}\right) \cdot 1h \end{aligned} \tag{4.28}$$

4.6. Phase-Change Material Thermal Energy Storage (PCM-TES) Model

4.6.1. Configuration

A thermal energy storage, based on phase-change materials (PCM-TES), can be integrated into the system to store the surplus energy produced by the heat pump with

respect to the heat demand of district heating. Conversely, in the winter months, when the heat pump capacity is insufficient, heat can be withdrawn from the TES to satisfy the demand. As for the other energy storage systems, also the PCM-TES is not designed in detail, the phase-change material is not selected and again only the maximum capacity and the loading/unloading efficiencies are assumed. The values are reported in Table 11 [7].

Table 11: PCM-TES features.

PCM-TES Features	Value
Maximum Capacity S_{max}	1000 kWh
Loading/Unloading Efficiency η_S	90%

4.6.2. Algorithm

The model describing the PCM-TES system is analogous to the ones previously presented for battery and BTES. Initially the energy stored in the PCM-TES is set to be 75% of the total capacity S_{max}. At every time iteration, the PCM-TES is either loaded or unloaded depending on the district heating demand and on the heat pump capacity ($D^{(k)}$ and $\dot{Q}_c^{(k)}$). During loading, the amount of thermal energy stored at the kth iteration is given by Equation 4.29.

$$\begin{aligned} S^{(k)} &= S^{(k-1)} + \eta_S \int_{t_{k-1}}^{t_k} \left(\dot{Q}_c - D\right) dt \\ &= S^{(k-1)} + \eta_S \left(\dot{Q}_c^{(k)} - D^{(k)}\right) \cdot 1h \end{aligned} \tag{4.29}$$

During unloading Equation 4.30 is used instead.

$$\begin{aligned} S^{(k)} &= S^{(k-1)} - (2 - \eta_S) \int_{t_{k-1}}^{t_k} \left(D - \dot{Q}_c\right) dt \\ &= S^{(k-1)} - (2 - \eta_S) \left(D^{(k)} - \dot{Q}_c^{(k)}\right) \cdot 1h \end{aligned} \tag{4.30}$$

4.7. District Heating Model

In this thesis, the district heating will not be modelled because the number and the type of building supplied with the heat produced by the heat pump are not decided upon. A mathematical expression is assumed for the heat demand composed of a water heating

and a space heating contribution (Equation 4.1). The whole district heating system will be treated as if it was a heat exchanger. At every time iteration, the hot water leaving the heat pump ceases the sensible heat defined by the heat demand to the district heating, returning to the heat pump condenser at a lower temperature. Hence, the temperature reduction of the hot water at the k[th] iteration can be calculated according to Equation 4.31.

$$\Delta T_{DH}^{(k)} = \frac{D^{(k)}}{m_{hw}^{(k)} c_p} \tag{4.31}$$

4.8. Integrated Energy System

4.8.1. Configuration

The integrated energy system is built by joining together all the subsystems presented in the previous Sections. The resulting plant scheme is shown in Figure 22. The heat pump

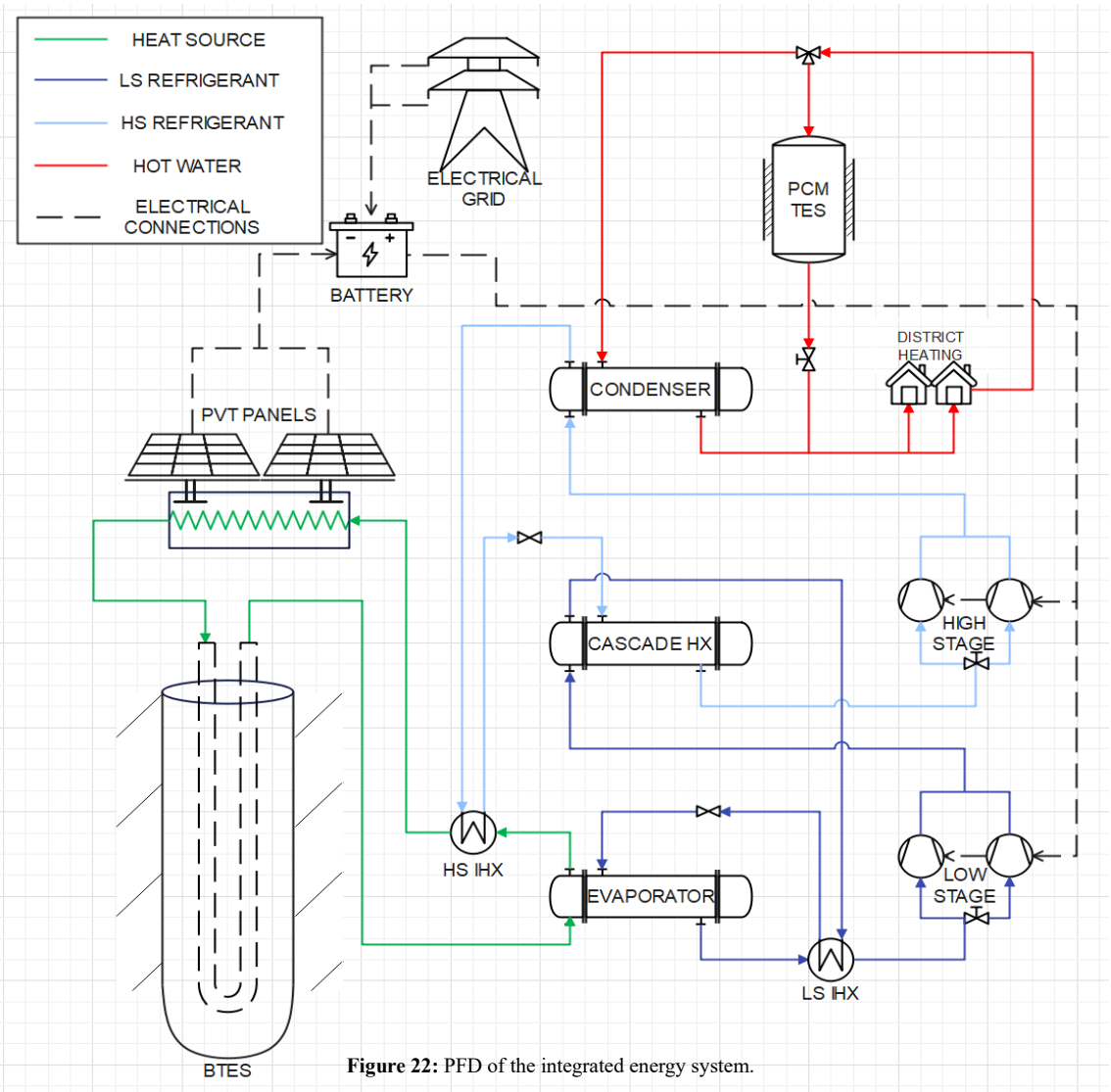

Figure 22: PFD of the integrated energy system.

has a double connection with the PVT panels. The first connection is thermal through the BTES, with which the heat source exiting the evaporator is re-heated in the PVT collector, before to return to the heat pump. The surplus or the deficit of thermal energy is either supplied or withdrawn from the BTES. The second connection is electrical through the battery accumulator. The electrical energy generated by the PVT collector is used to drive the heat pump compressors. When a surplus or deficit of electrical energy results, the battery is either charged or uncharged. Moreover, the heat pump has a thermal connection with the district heating via the PCM-TES. Similarly to the previous cases, the hot water produced by the heat pump is supplied to the district heating, then returned to the heat pump condenser at a lower temperature. If the heat demand overcomes the condenser capacity, the remaining part of thermal energy is furnished by the PCM-TES, otherwise the thermal energy surplus is stored. A connection to the external electrical grid is present, the system can either import or export electrical energy to the outside when the battery capacity is minimal or maximal respectively.

4.8.2. Algorithm

The integrated energy system works according to an algorithm that combines all the models developed for the subsystems in the previous sections. First the weather data (air temperature and solar irradiance) on an hourly basis specific for Oslo in year 2005 are retrieved. From there it is possible to calculate heat demand for district heating, electrical and thermal power generation from the PVT panels throughout the year. The system is then initialized. For battery, BTES and PCM-TES the initial values of capacity are set to be 75% of the maximum. For all the time iteration, namely from the first to the last hours of year 2005, many system parameters are calculated: heat pump operational mode, condenser and evaporator capacities, power consumption, battery stored energy, BTES stored energy, PCM-TES stored energy, power imported or exported to the electrical grid and heat supplied to district heating. At the beginning of an iteration, if the PCM-TES is at its maximum capacity, the heat pump is shut-off, because the thermal energy surplus produced would be wasted. In that case the heat demand is satisfied with the solely heat stored in the PCM-TES. Both capacities and power consumption are null, thus battery and BTES are loaded. If thermal energy can still be stored in the PCM-TES, then the operational mode of the heat pump at that time iteration is decided depending on the available electrical energy (power generated by the PVT panels plus energy stored in the

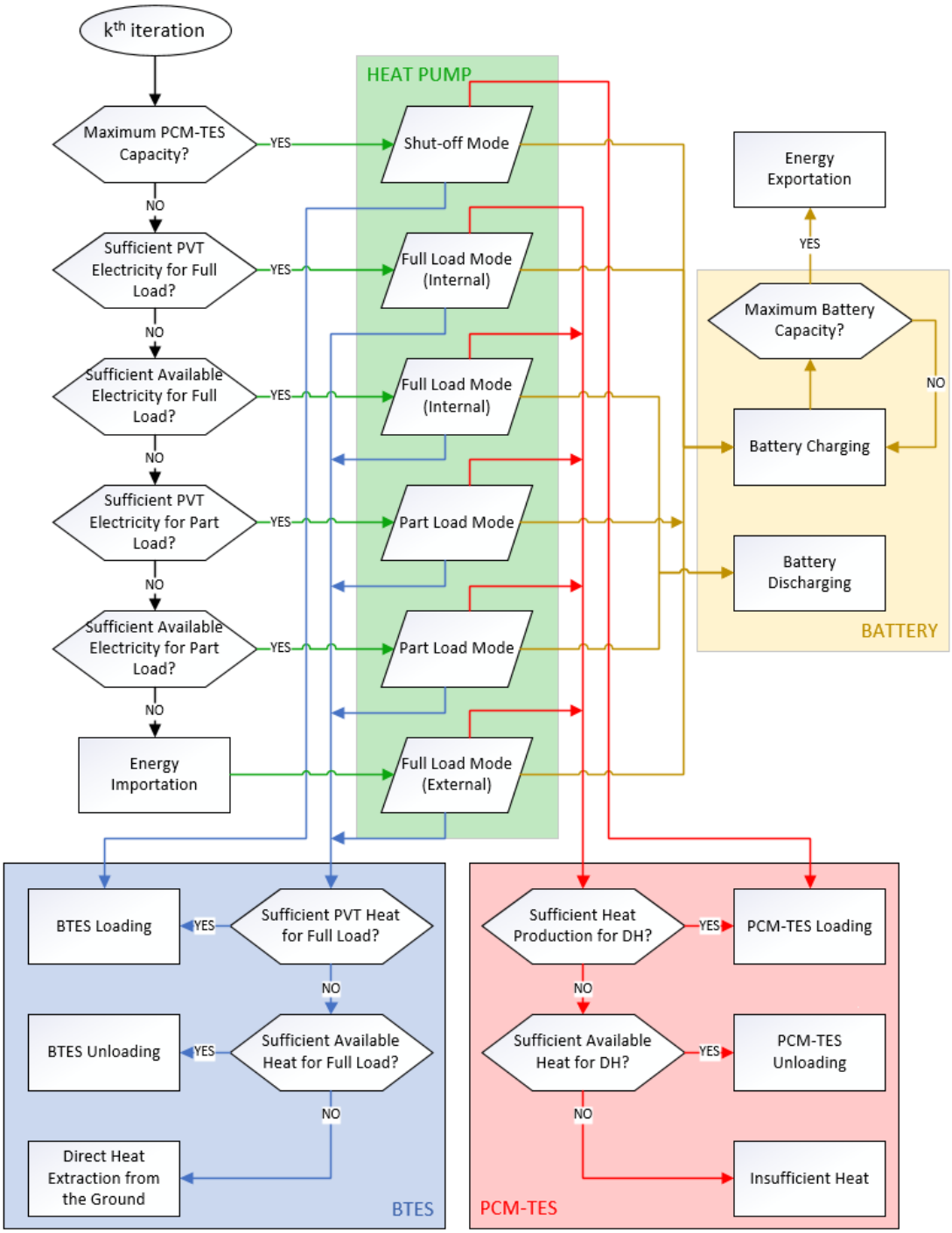

Figure 23: BFD of the algorithm used to simulate the integrated energy system (the sections are highlighted with different colors).

battery). If the available electrical energy is sufficient, the heat pump runs on full load, and the battery can be either charged or uncharged. Otherwise, if the available electrical energy is enough to run the heat pump on part load, said operation is selected and again the battery can either be charged, when surplus electrical energy is produced, or uncharged instead. If at a certain iteration there is not enough available energy to run the heat pump on part load, energy is imported from the external and the heat pump is run on

full load, charging the battery too. Every time the battery is charged, the maximum capacity might be reached, in that case the electrical energy that cannot be stored is exported to the outside through the electrical grid. When the BTES reaches its maximum capacity, then the thermal energy that would be added is assumed to be completely wasted. On the other hand, when the BTES reaches its minimum capacity, the heat source is assumed to be re-heated to 40°C, regardless of the thermal energy missing. Finally, when the PCM-TES reaches its maximum, the heat pump is shut-off to avoid thermal energy dissipation. Figure 23 shows the BFD of the integrated energy system algorithm.

5. Results

5.1. Yearly Results

The results obtained through the Matlab code bult for modelling the integrated energy system are presented in this chapter on a yearly basis. However, due to the very high number of time iterations (8760), the results displayed in a plot may be difficult to interpret. Results specific for winter, summer, and spring/fall are presented separately in the following chapters to facilitate both visualization and discussion.

5.1.1. Air Temperature and Solar Irradiation

From the weather data obtained using Meteonorm, the plot shown in Figure 24 can be obtained by averaging the air temperature and solar irradiance for every week. The average temperature between winter and summer varies significantly: the air temperature usually remains above 15°C during the summer and between 0 and -5°C during the winter.

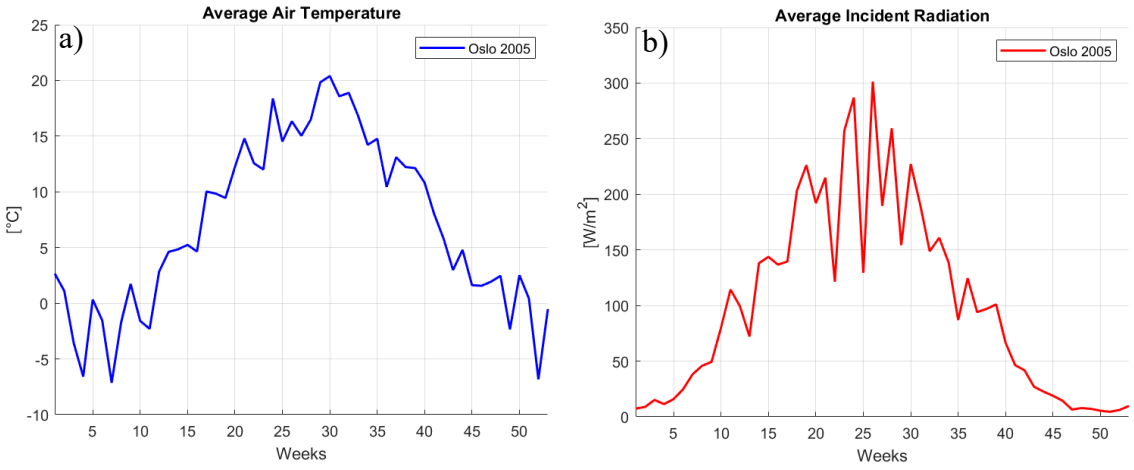

Figure 24: Weekly averaged air temperature (**a**) and solar irradiance (**b**) in Oslo during the year 2005.

The average solar irradiance shows an extreme variation during the year. This is due to the high latitude of Oslo, which ensures more than 200 monthly sunshine hours in the summer, but only 50 during the winter [47]. Since the average trend is shown, the local maxima and minima of temperature cannot be seen in Figure 24a. They are shown in Table 12. Because both air temperature and solar irradiance vary from year to year, they might not be accurate for 2024 or later years. Nevertheless, according to Michaels et al. [48], yearly temperatures follow trends and the average temperatures in each month rarely vary with more than two degrees; thus, the values are assumed to be representative for the simulation at this point in the project.

Table 12: Maximum, minimum and average air temperature in Oslo during the year 2005.

Descriptor	Air temperature	Solar Irradiance
Maximum	+29.8°C	868 kW/m^2
Minimum	-13.3°C	0 kW/m^2
Winter Average	-1.9°C	35 kW/m^2
Summer Average	+15.9°C	166 kW/m^2
Yearly Average	+7.1°C	102 kW/m^2

5.1.1. Integrated Energy System Performance

The simulation of the integrated energy system for the whole year gives results in terms of the performance of all the subsystems. For what concerns the heat pump, it can run on

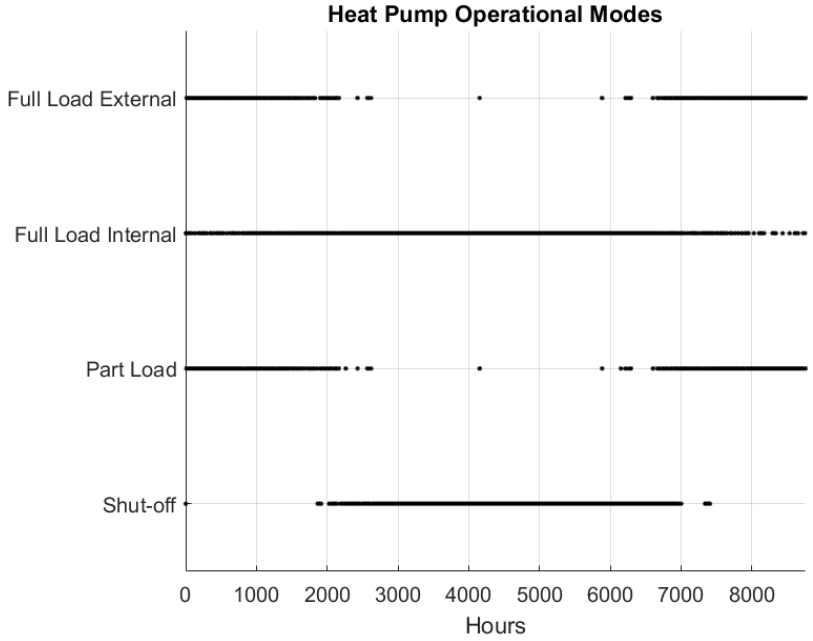

Figure 25: Heat pump operational modes during the year.

Table 13: Hours of full load, part load and shut-off operation in different periods of the year.

Period	Hours Full Load		Hours Part Load	Hours Shut-off
	Internal	External		
January	53 (7.2%)	370 (49.7%)	321 (43.1%)	0 (0.0%)
April	540 (75.0%)	14 (1.9%)	13 (1.8%)	153 (21.3%)
July	380 (51.1%)	0 (0.0%)	0 (0.0%)	364 (48.9%)
October	220 (29.5%)	217 (29.2%)	197 (26.5%)	110 (14.8%)
Year	3497 (39.9%)	1770 (20.2%)	1540 (17.6%)	1953 (22.3%)

three different operational modes, depending on the overall energy availability and demand of the system. The trend with which the operational mode is changed during the year is shown in Figure 25. The quantification of the hours in each mode, also divided for specific periods of the year, is reported in Table 13.

For the sake of clarity, a distinction has been made between the system's full load operation driven by the directly available electrical energy (internal full load) and the full load operation driven by the electrical energy provided by the external grid (external full load). The heat pump works on full load for the whole year, but it alternates its operational mode with the part load mode roughly during the winter, or with the shut-off mode in the warm months. In the winter the full load operation of the heat pump is mainly sustained by the external grid. In the spring and in the summer the system does not rely heavily on the grid, while in the fall it is equally driven by the power generated by the PVT panels and the power imported from the external grid.

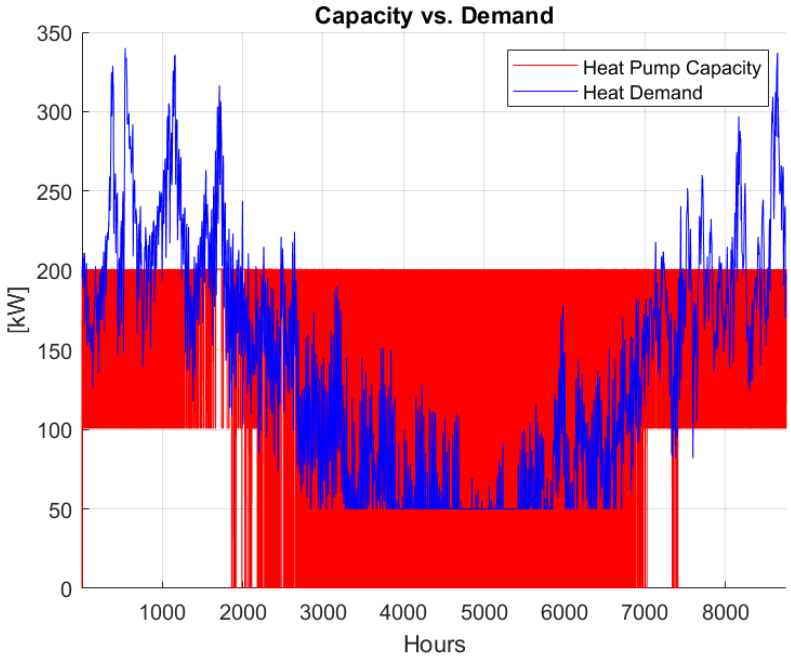

Figure 26: Heat pump capacity and heat demand during the year.

In Figure 26 the heat capacity of the heat pump is displayed together with the heat demand of district heating, the three operational modes of the heat pump are clearly distinguishable. The full load supplies 200 kW, the part load supplies 100 kW, while in shut-off mode the capacity is null. The heat demand highly exceeds the full load capacity of the heat pump in the winter months, the maximum heat demand of 340 kW is attained when the air reaches its minimum temperature on January 22nd. In the summer the heat

demand rarely surpasses 100 kW, therefore the heat pump can always deliver sufficient heat to district heating.

The total thermal energy produced weekly by the heat pump is shown in Figure 27. It is higher in the winter and always above 25 MWh per week, with a peak of 33 MWh. It is lower in the summer and maintains an energy production between 15 and 20 MWh.

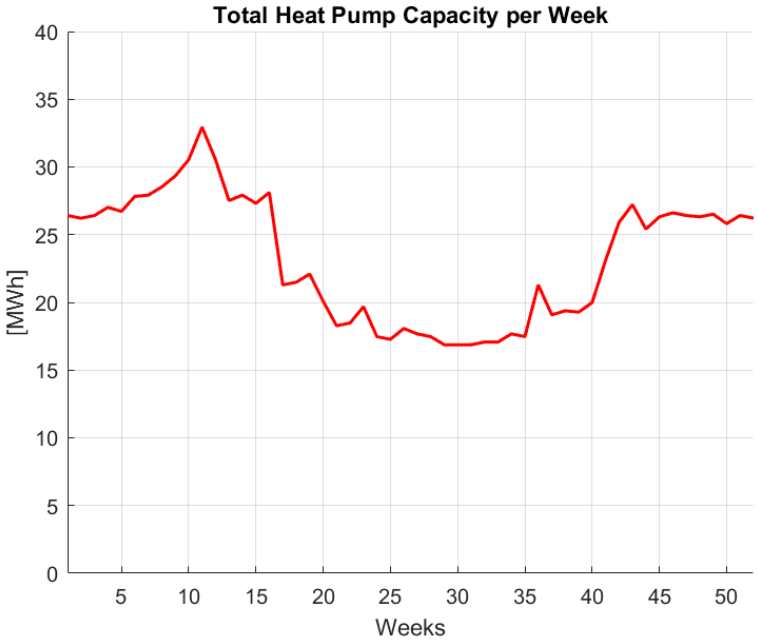

Figure 27: Total heating capacity generated by the heat pump per week.

In Figure 28 the weekly averaged heat demand is compared to the weekly averaged heat available for district heating. The availability of heat, namely the one stored in PCM-TES

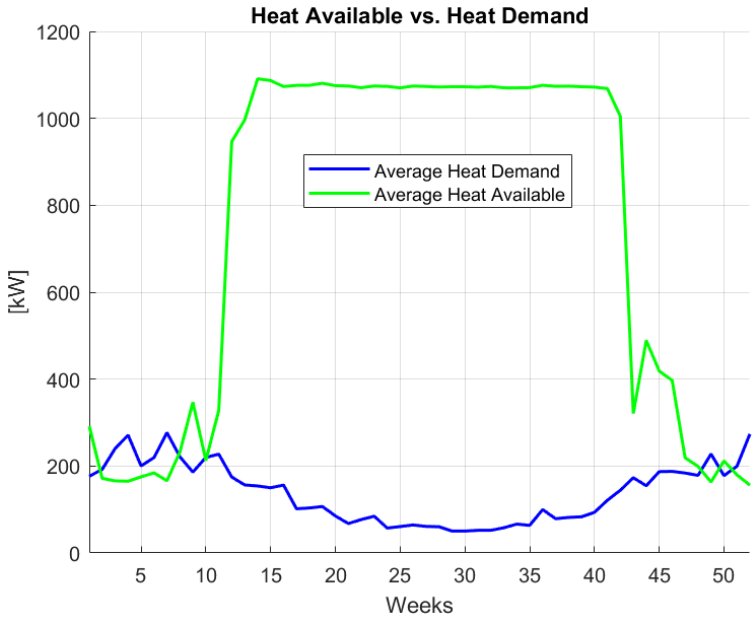

Figure 28: Weekly averaged heat demand and heat available during the year.

plus the one produced on time by the heat pump, is always much higher than the demand in the summer, and in large part of spring and fall. In the winter, on the other hand, there are few weeks during which the heat demand surpasses the heat available. The results shown in Figure 28 are quantified in Table 14, in terms of number of hours of insufficient heat and amount of insufficient heat.

Table 14: Hours and total amount of insufficient heat in different periods of the year.

Period	Hours Insufficient Heat	Total Insufficient Heat [MWh]
January	538 (72.3%)	49.02
April	0 (0.0%)	0.00
July	0 (0.0%)	0.00
October	80 (10.8%)	4.80
Year	2242 (25.6%)	183.73

Taking January as a reference for the winter months, for 72.3% of the integrated energy system operation, the heat available is insufficient to fulfill the district heating demand. Only in the month of January, 49.02 MWh of thermal energy has not been delivered. Overall, one quarter of the year is characterized by insufficient heat, which sums up to a total lack of 183.73 MWh.

Table 15: Total electrical energy produced by the PVT panels and consumed by the heat pump for various periods of the year.

Period	Total Energy Produced by the PVT Panels [MWh]	Total Energy Consumed by the Heat Pump [MWh]
January	4.67	37.86
April	60.81	36.45
July	96.62	24.71
October	19.00	34.81
Year	547.48	392.56

Results specific to the production and consumption of electrical energy are reported in Table 15. During the winter, little energy is produced by the PVT collector, due to the short duration of the days, with a total energy consumption of the heat pump that is more than 8 times larger. Conversely, in the month of July, 20 times more electrical energy is generated by the PVT panels than in January and with a lower consumption by the heat pump. Considering the whole year, 72% of the electrical energy deriving from the sun is

spent to drive the heat pump. The remaining part is either exported to the grid or wasted due to the charging/discharging efficiency of the battery.

The results concerning the thermal energy production by the heat pump and the delivery to district heating are shown in Table 16. In the winter all the heat produced is supplied to the district heating and a small part is wasted due to the loading/unloading efficiency of the PCM-TES. During the summer only 54% of the heat is delivered. The remaining part is stored in the PCM-TES, again with a certain efficiency.

Table 16: Total heat produced by the heat pump and supplied to district heating for various periods of the year.

Period	Total Heat Produced by the Heat Pump [MWh]	Total Heat Supplied to District Heating [MWh]
January	116.57	116.45
April	112.18	101.21
July	76.06	41.38
October	107.17	99.14
Year	1208.24	1040.03

The amount of energy (electrical and thermal) lost by loading and unloading the accumulators (battery, BTES, PCM-TES) is investigated too. The results are reported in Table 17. The battery is the accumulator that is wasting the biggest amount of energy, but it is also the one having the lowest loading/unloading efficiency, i.e. 80%. Most of the electrical energy loss occurs in April, while in winter and summer the loss is lower. The thermal energy loss caused by the BTES does not show a large variability during the year, it is slightly higher in the cold period. Conversely, the thermal energy loss caused by the PCM-TES is very low in the month of January and higher in the warm period.

Table 17: Total energy lost by the accumulators (Battery, BTES and PCM-TES) for various periods of the year.

Period	Energy Lost by the Battery [MWh]	Energy Lost by the BTES [MWh]	Energy Lost by the PCM-TES [MWh]
January	4.87	6.73	0.88
April	9.30	4.77	4.17
July	4.91	4.74	4.19
October	6.02	7.00	3.89
Year	72.01	51.27	37.81

The last outcome deriving from the simulation of the integrated energy system is the import/export of electrical energy from/to the grid. The results are shown in Table 18. Most of the importation of external energy occurs during the winter, when the exportation is null. In the fall the amount of energy imported is higher than the one exported, while in the spring the opposite is true. Eventually, in the summer, no electrical energy is imported from the grid, a substantial exportation takes place instead. Considering the whole year, the balance between exportation and importation is positive, with a net production of 85 MWh.

Table 18: Total electrical energy imported and exported to the grid for various periods of the year.

Period	Total Energy Imported from the Grid [MWh]	Total Energy Exported to the Grid [MWh]
January	36.90	0.00
April	1.40	15.79
July	0.00	67.03
October	21.70	0.91
Year	177.00	262.77

5.2. Winter Results

The results of the integrated energy system simulation specific for the wintertime are presented for the month of January, taken as a reference winter month. The heat pump is the core of the integrated energy system and it has two energy inlets: a thermal and an electrical one. Additionally, it has one thermal energy outlet; each input/output contains an energy production, an energy storage and an energy consumption subsystem.

The results for the electrical input comprise the electrical PVT generation, the battery storage and the compressors consumption of the heat pump. They are shown in Figure 29. During January little electrical energy is produced by the PVT solar collector. Rarely the power generated by itself is sufficient to sustain the heat pump, whose power consumption oscillates between 32 and 65 kW. The initial battery capacity is 750 kWh (75% of the maximum), and runs out in a few hours by feeding the heat pump; then the capacity never exceeds 60 kWh for the whole month of January.

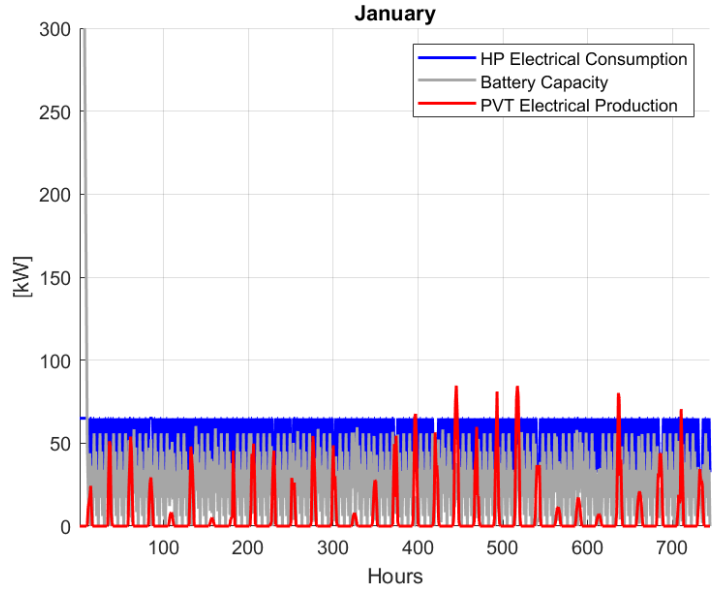

Figure 30: Trends of heat pump consumption, battery capacity, and PVT production of electrical energy in January.

Figure 30 shows the results of the thermal input of the integrated energy system. Two y-axes are present for helping with the visualization.

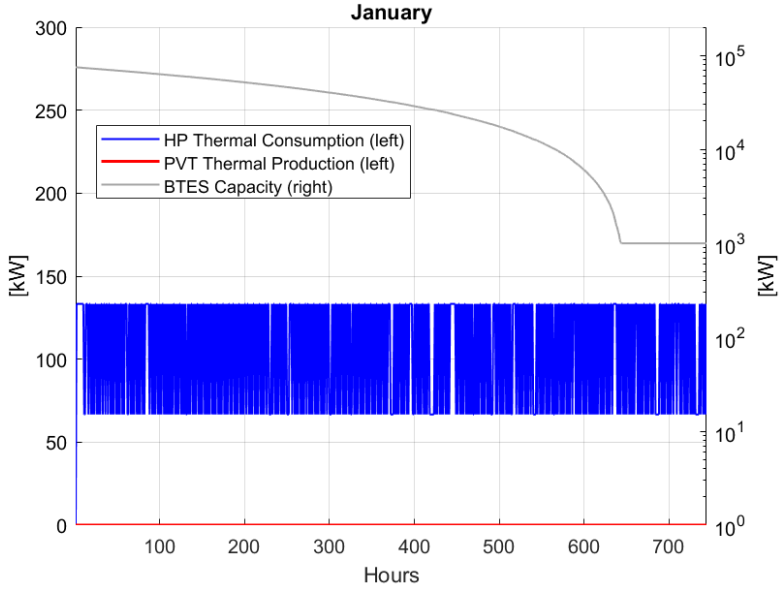

Figure 29: Trends of heat pump consumption, BTES capacity, and PVT production of thermal energy in January.

The thermal energy produced by the PVT panels is null for the whole month of January. In fact the air temperature is too low, and does not result in a positive thermal efficiency of the PVT collector. The heat pump is therefore thermally driven only by the heat stored in the BTES, which initially is 75 MWh (75% of the maximum), then decreases rapidly until reaching the 1% capacity before the end of January and simultaneously remains constant, since a continuous 1 MW of thermal energy is supplied by the ground.

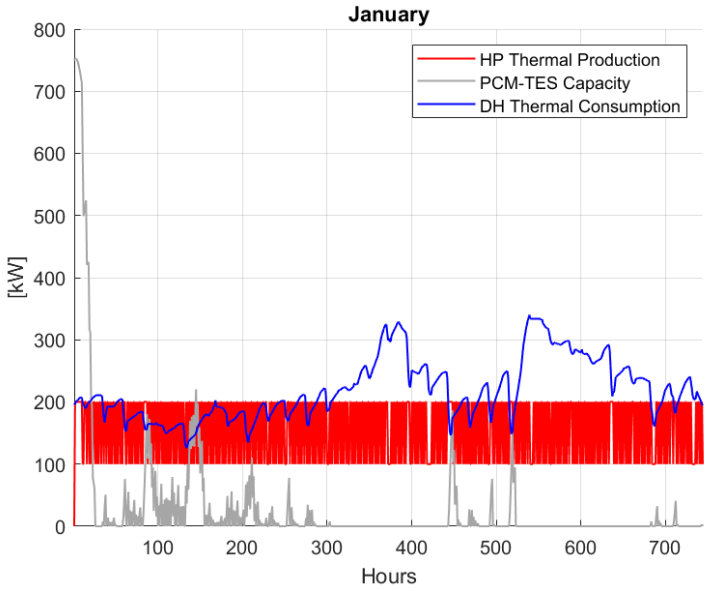

Figure 31: Trends of district heating consumption, PCM-TES capacity, and heat pump production of thermal energy in January.

The trends specific for the thermal energy outlet of the overall system, namely district heating consumption, PCM-TES capacity, and heat pump generation, are shown in Figure 31. In the first part of January, the heat demand is comparable with the full load capacity of the heat pump. After half of the month it increases, exceeding 300 kW for some hours. The PCM-TES capacity initially is 750 kWh (75% of the maximum), but, since the part load operation is adopted many times, the heat available in the storage is drained rapidly. A small amount of heat is stored in the PCM-TES during the short periods when the heat demand remains lower than the heat supplied by the heat pump.

5.3. Summer Results

July is the reference month for the summertime operation of the integrated energy system. The presentation of the summer results is made according to the system's input/output structure, starting with the electrical energy input. Figure 32 shows the trends of PVT generation, battery capacity, and heat pump electrical consumption.

Thanks to the longer daylight period and stronger solar irradiance during the month of July, the PVT collector produces much more electrical energy than in the winter. The production has spikes of 500 kW, allowing the battery to be completely full for many hours. The heat pump is alternatively on full load mode or shut-off. The active operation is sustained by the battery during the night. Due to bad weather conditions over five to

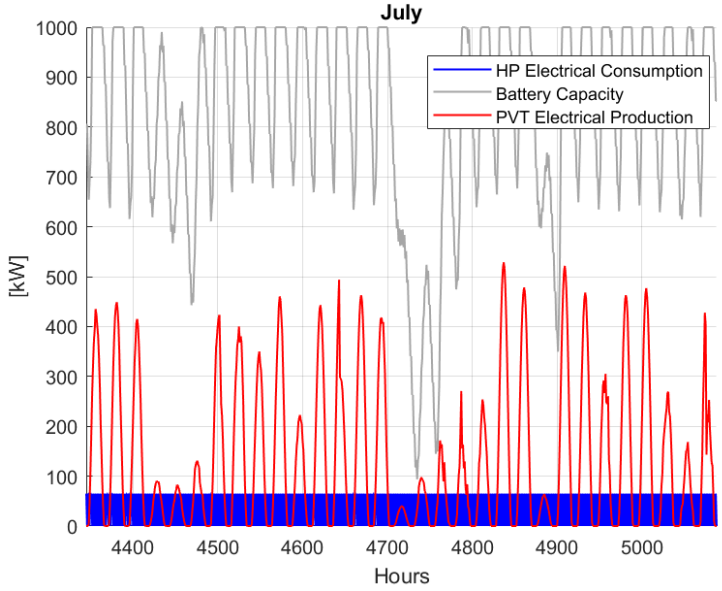

Figure 32: Trends of heat pump consumption, battery capacity, and PVT production of electrical energy in July.

six days the production does not reach 100 kW. Correspondingly, the battery capacity drops down significantly, but it is not drained completely.

The results specific for the thermal energy input in the month of July are shown in Figure 33, two different y-axes are used for a better visualization. Like the electrical case, the production of thermal energy by the PVT collector is much higher in the summer than in winter. In the warmer days, with high solar irradiance, there are peaks in production up to 1500 kW. In July, apart from a few days, the full load thermal energy requirement of the heat pump is always at least six to eight times smaller than the heat production of the PVT panels. Consequently, the BTES capacity never gets below 90% of its maximum.

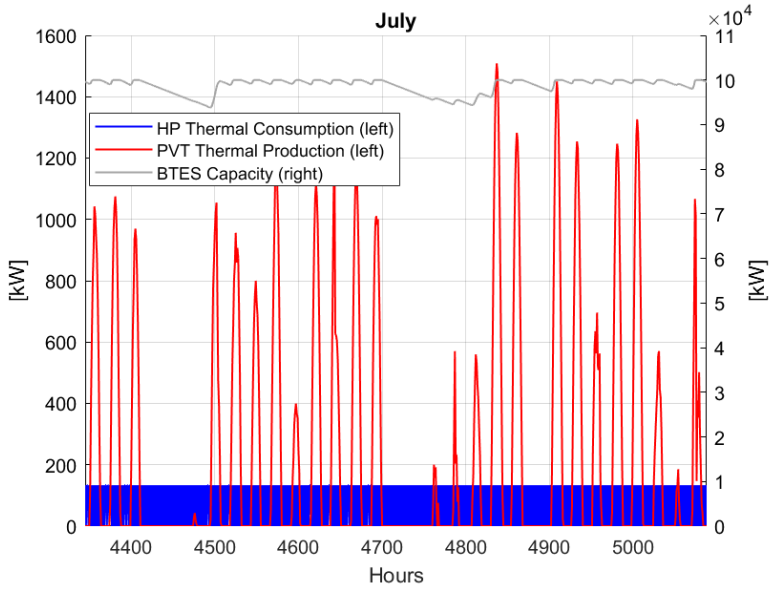

Figure 33: Trends of heat pump consumption, BTES capacity, and PVT production of thermal energy in July.

At last the results for the thermal energy output are displayed in Figure 34. As already shown many times, the heat demand for district heating in the summer is much lower than in the winter. Particularly in July, it is rarely higher than the minimum of 50 kW. The PCM-TES capacity is often at the maximum and the heat pump is shut-off quite frequently. When the heat pump is operating on the other hand, it works on full load mode, always delivering more than twice the demand of heat.

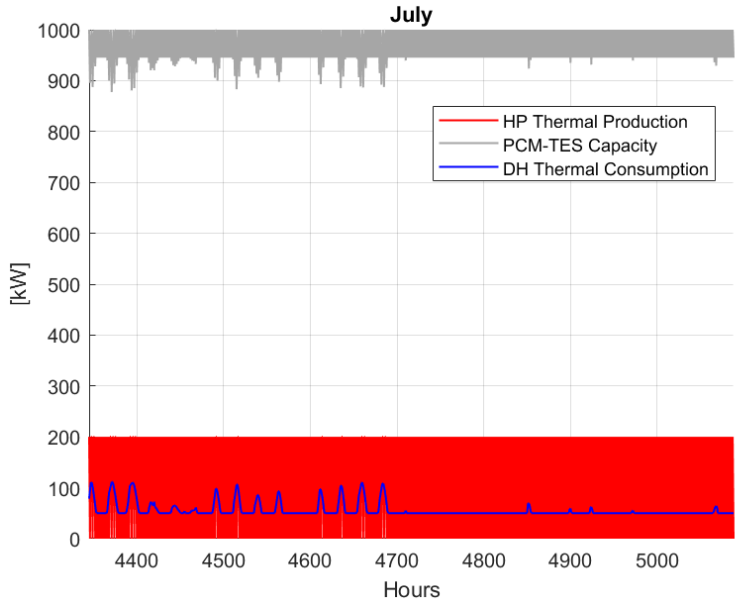

Figure 34: Trends of district heating consumption, PCM-TES capacity, and heat pump production of thermal energy in July.

5.4. Spring/Fall Results

The outcome of the simulation for both spring and fall periods are summarized in the results obtained in the month of April (see Figures 35-37).

The production of electrical energy by the PVT collector is intermediate between the winter and summer ones, and the battery capacity continuously oscillates between full capacity and 30-40% of the maximum. The production of thermal energy presents some isolate peaks of power that are not as high as the summer ones, to which correspond peaks of BTES capacity. The heat pump alternates its operation on all the possible modes during the month of April, and generally the full load operation can provide enough heat to satisfy the heat demand of district heating. To conclude, the capacity of the PCM-TES remains always close to the maximum, it experiences some negative peaks mainly correlated to the shut-off mode.

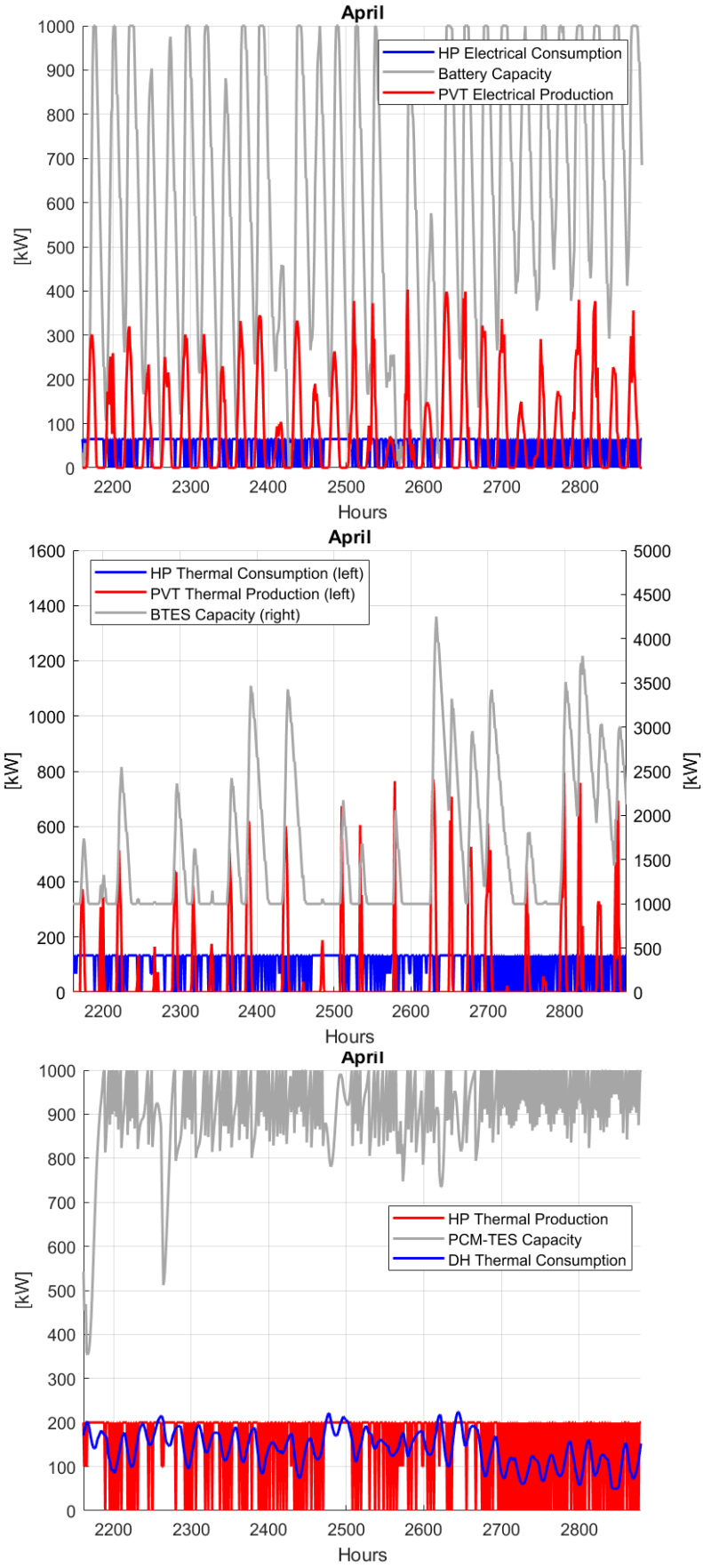

Figures 35-37: Trends of the parameters characterizing the integrated energy subsystems in April.

5.5. Increased Battery Efficiency

The simulation of the IES is repeated with a higher efficiency of the battery. Rather than consider the charging/discharging efficiency, the round-trip efficiency (RTE) is taken into account. The RTE is the percentage of electrical energy that is lost during a battery charge/discharge cycle. According to Noyanbayev et al. [49], for a lithium-ion battery, the RTE corresponding to a full charge-discharge cycle is around 90%. Equations 4.25 and 4.26 are modified, incorporating the definition of RTE, obtaining Equations 5.1 and 5.2 for charging and discharging respectively.

$$B^{(k)} = B^{(k-1)} + \eta_B^* \int_{t_{k-1}}^{t_k} \left(\dot{P}_{el} - \dot{W}_c\right) dt = B^{(k-1)} + \eta_B^* \left(\dot{P}_{el}^{(k)} - \dot{W}_c^{(k)}\right) \cdot 1h \quad (5.1)$$

$$B^{(k)} = B^{(k-1)} - \int_{t_{k-1}}^{t_k} \left(\dot{W}_c - \dot{P}_{el}\right) dt = B^{(k-1)} - \left(\dot{W}_c^{(k)} - \dot{P}_{el}^{(k)}\right) \cdot 1h \quad (5.2)$$

Where η_B^* is the round-trip efficiency. The effect of the RTE is accounted only for the charging phase. The number of hours for each operational mode changes, the new results are reported in Table 19, together with the ones showed in Table 13.

Table 19: Comparison of the operational mode distribution in different periods of the year, with the new efficiency.

Period	Hours Full Load		Hours Part Load	Hours Shut-off
	Internal	External		
January	53 → 56	370 → 324	321 → 364	0 → 0
April	540 → 553	14 → 5	13 → 7	153 → 155
July	380 → 380	0 → 0	0 → 0	364 → 364
October	220 → 251	217 → 178	197 → 205	110 → 110
Year	3497 → 3661	1770 → 1504	1540 → 1639	1953 → 1956

A higher battery efficiency increases the number of hours in which the heat pump is operated on internal full load and part load modes, with the detriment to the external full load mode. These trends can be noticed mainly in winter, spring and fall, in July no change in the distribution is present.

In terms of heat delivered to district heating, the results of the IES with the new battery efficiency are displayed in Table 20, together with the ones showed in Table 14.

Table 20: Comparison of hours and total amount of insufficient heat in different periods of the year, with the new efficiency.

Period	Hours Insufficient Heat	Total Insufficient Heat [MWh]
January	538 → 563	49.02 → 53.18
April	0 → 0	0.00 → 0.00
July	0 → 0	0.00 → 0.00
October	80 → 100	4.80 → 6.27
Year	2242 → 2309	183.73 → 195.37

The number of hours in which the heat pump delivers an insufficient amount of heat to district heating increases slightly during winter and fall. This is due to the fact that the heat pump operates more frequently in part load mode, thus it produces less thermal energy.

Finally, the energy saved with a higher battery efficiency can be calculated and a comparison can be done between the amounts of electricity imported and exported to the grid before and after the increase in efficiency. The results are reported in Table 21, together with the ones showed in Tables 17 and 18.

Table 21: Comparison of energy lost by the battery, imported and exported in different periods of the year, with the new efficiency.

Period	Energy Lost by the Battery [MWh]	Total Energy Imported from the Grid [MWh]	Total Energy Exported to the Grid [MWh]
January	4.87 → 1.21	36.90 → 32.30	0.00 → 0.00
April	9.30 → 2.17	1.40 → 0.50	15.79 → 21.92
July	4.91 → 1.08	0.00 → 0.00	67.03 → 70.85
October	6.02 → 1.52	21.70 → 17.80	0.91 → 1.50
Year	72.01 → 17.46	177.00 → 150.40	262.77 → 292.05

The electrical energy lost by the battery strongly decreases, by more than 75%. The IES requires now 15% less electricity to be imported from the grid, while it can export 11% more.

6. Discussion

6.1. Integrated Energy System Design

The IES has been built mathematically by merging the models describing its subsections. Starting from the heat pump, it has been modelled with the highest degree of detail and the "lightest" assumptions. The zeotropic mixtures selected for high and low stage provide the best coupling between each other and with the heat source and sink, this was confirmed by the LMTD profiles in the heat exchangers. The heat pump was sized according to the amount of thermal energy to be supplied for district heating. Its model provides steady-states results of the operation in terms of energy input and output in two operational modes: full load and part load. Finally, the energy integration procedure enabled the COP to reach 3.6, fulfilling the design specifications imposed. For the other parts of the IES a sizing approach was not used, the size parameters were simply assumed based on previous researches. The sections are combined with an algorithm which regulates the supply of heat with respect to the demand and to the available power.

6.2. Seasonal Variations

The operational mode distribution of the heat pump changes significantly between summer and winter. During the winter the heat pump switches continuously between full load externally driven and part load mode. In the cold months there is little solar irradiance during the day, insufficient to drive the compressors and charge the battery. Electrical power is therefore imported from the grid, allowing the heat pump to work at full load and charge the battery at the same time. Then the heat pump operates at full load until the battery is full enough to sustain the part load operation or until the PVT collector produces enough electrical energy. Conversely, during summer the heat pump oscillates between internally driven full load and shut-off modes. The shut-off operation is programmed to activate when the PCM-TES is at its full capacity. This happens when the heat demand is low, in the summer it remains around the minimum of 50 kW most of the time. The solar irradiance is usually high enough to ensure the full load operation during the day, while in the night the battery is discharged to fulfill the energy requirements of the heat pump.

The total heat delivered is the highest during winter because the heat pump is never shut-off, hence heat production is continuous. In summer the heat pump often is not active, because the low demand can be satisfied by the heat stored in the PCM-TES. Considering now the heat available, it remains stationary at around 1,100 kW during the warm months. The heat production is 200 kW at full load, 1,000 kWh are stored in the PCM-TES usually full, while the heat demand to be subtracted is between 50 and 100 kW. Vice versa, in the winter the heat pump keeps switching between 200 kW and 100 kW of heat production, and the PCM-TES frequently runs low capacity. This explains why there is insufficient heat production in the cold months.

6.3. Energy Efficiency

The IES is not 100% efficient, a certain energy efficiency is associated to each section of the plant. Specifically, the PVT collector is characterized by electrical and thermal efficiencies of conversion of solar energy, both varying along time. The electrical efficiency during the day is around 14%, which is a reasonable value for commercial solar cells. As showed previously, the thermal efficiency is null during the winter days, due to the too low air temperature and solar irradiation; while it can reach 45% in the warmest days.

Conversely, for the three energy storages a fixed energy efficiency is defined, specific for the loading/unloading step. The PCM-TES is loaded with the heat resulting from the difference between heat pump capacity and heat demand. In winter rarely the PCM-TES gets rarely loaded, while in the summer it is often at full capacity. It follows that the heat lost by the PCM-TES is higher when the cycles loading/unloading are more frequent, this happens in spring and fall. Similarly happens for BTES and battery.

In the specific case of the battery accumulator, the round-trip efficiency can be considered rather than the charging/discharging efficiency. Results showed that the electricity loss decreases significantly, but at the same time the hours of insufficient heat supply increased. The distribution of the HP operational modes changed during both summer and winter.

6.4. Energy Independency

A positive balance between exportation and importation of electrical energy from the grid means that, despite energy losses, the system can sustain its operation during the year. However, during winter, the system cannot rely only on the solar energy. Particularly in a Nordic country as Norway, a connection with the electrical grid is essential. The importation of energy from the grid decreases significantly when considering a higher battery efficiency. Due to the very low thermal efficiency, the PVT collector does not produce thermal energy during the winter. A huge underground heat storage is required, which might be an unfeasible solution for the high cost and construction difficulty. An alternative renewable energy source needs to be considered for fulfilling the thermal energy requirement of the heat pump during the cold period. Nevertheless, PV panels with thermal integration coupled with one or more boreholes is an optimal solution in the summer, because the solar energy can be converted into heat with a good efficiency. Subsequently the heat surplus can be stored in the ground without the need of large storage facilities on the surface.

7. Conclusions

In this thesis an integrated energy system has been built and its performances evaluated, as part of the bigger research project ChiNoZEN. The network comprises photovoltaic/thermal (PVT) panels, a borehole thermal energy storage (BTES), a battery, a phase-change material thermal energy storage (PCM-TES), a district heating (DH) section, and a cascade high temperature heat pump (HTHP) which uses zeotropic refrigerants and represents the core of the plant. The system was simulated using Matlab, with weather data retrieved from Meteonorm. The selected location was Oslo, in the reference year 2005. Operation and performance of all the subsystems have been investigated for every hour along the whole year. The results obtained from the steady-state simulation of the heat pump were excellent. Hot water at 100°C can be produced and delivered for district heating, with a temperature lift of 80°C. The cascade cycle has a very high energy efficiency, with a COP of 3.6. Due to the high variability of the atmospheric conditions during the year, a huge difference between winter and summer operation was highlighted. In the warm months, the heat pump is frequently shut-off because the heat demand is low, and the PCM-TES is usually at full capacity. Conversely, in the winter, the heat pump operates often on full capacity driven by external electricity from the grid. The PVT collector is not able to provide enough electrical and thermal energy due to the short duration of the winter days. Overall, the system self-sustains its operation. In winter, some external electric power is required to drive the heat pump; but it is completely compensated in the summer season, resulting in a positive balance.

The integration of cascade high-temperature heat pumps within an IES presents a promising avenue for sustainable and efficient energy utilization. The synergistic coupling of different temperature levels in the cascade system has proven to be a pivotal factor, enabling the harnessing of thermal energy across a broader spectrum. Through this comprehensive study, the multiple benefits of this innovative approach have been elucidated. In essence, the integration of cascade HTHPs into the energy infrastructure represents a promising option for a more sustainable and resilient energy future.

As we move forward, it is imperative to consider further research and development to refine the technology, address any challenges that may arise during implementation, and to explore opportunities for wider adoption. There are several aspects that need to be

improved from the model in this thesis. The heat pump model should be updated considering the actual variations in the temperature of the water entering the heat exchangers; thus, a transient simulation should be performed rather than a steady-state one. The models for the PVT system and district heating system need to be updated. The return temperature of both hot water and heat source should be thoroughly regulated and the mass flow rates of water and refrigerant should be adjusted to various scenarios. The sizes of various components such as heat exchanges and compressors should be optimized to improve the COP. The energy consumed by each side equipment constituting the heat pump should be calculated, rather than just the power consumption of compressors. Considering now the IES, its subsections should be sized based on the amount of energy to be produced or stored in them. Additionally, other renewable energy sources need to be considered, since the PVT collector cannot convert solar energy into heat during winter. From the financial point of view, an economic assessment should be performed. The capital cost of every part of the system must be estimated then, together with operative costs and revenues, the payback period can be calculated. With this last result, it will be possible to tell if the capital investment is profitable or not. Eventually, a deeper work on the system can be conducted, building a pilot plant of the HP to obtain experimental results and validate the theoretical study.

References

[1] IEA, «Energy Statistics Data Browser,» 21 12 2023. [Online]. Available: https://www.iea.org/data-and-statistics/data-tools/energy-statistics-data-browser. [Consultato il giorno 17 01 2024].

[2] United Nations, «The 17 Goals,» [Online]. Available: https://sdgs.un.org/goals. [Consultato il giorno 17 01 2024].

[3] European Commission, «Climate Action,» [Online]. Available: https://climate.ec.europa.eu/index_en. [Consultato il giorno 18 01 2024].

[4] United Nations, «The Paris Agreement,» [Online]. Available: https://unfccc.int/process-and-meetings/the-paris-agreement. [Consultato il giorno 18 01 2024].

[5] NTNU, «About ChiNoZEN,» [Online]. Available: https://www.ntnu.edu/ept/chinozen#/view/about. [Consultato il giorno 19 12 2023].

[6] S. T. Ryssdal, «High Temperature Heat Pumps in Integrated Energy Systems,» 2020.

[7] S. Skoglund, «High Temperature Heat Pumps Using Zeotropic Refrigerant in Integrated Energy Systems,» 2022.

[8] P. Ganesan e T. M. Eikevik, «New zeotropic CO2-based refrigerant mixtures for cascade high-temperature heat pump to reach heat sink temperature up to 180 °C,» *Energy Conversion and Management: X,* vol. 20, 2023. DOI: 10.1016/j.ecmx.2023.100407

[9] P. Ganesan, T. M. Eikevik, K. Hamid, R. Wang e H. Yan, «Thermodynamic analysis of cascade high-temperature heat pump using new natural zeotropic refrigerant mixtures: R744/R600 and R744/R601,» *International Journal of Refrigeration,* vol. 154, pp. 215-230, 2023. DOI: 10.1016/j.ijrefrig.2023.05.017

[10] R. Slack, M. Tomlin, J. Barrett e J. Nonweiler, «Optimized Heat Pump System». Europe Brevetto EP 3 196 559 A1, 26 07 2017.

[11] A. Olympios, M. Mersch, P. Hoseinpoori e A. M. Pantaleo, «Optimal design of low-temperature heat-pumping technologies and implications to the whole-energy system,» 2020.

[12] L. G. Hays, «High temperature heat pump». USA Brevetto US 6 913 076 B1, 05 07 2005.

[13] O. Bamigbetan, T. M. Eikevik, P. Nekså, M. Bantle e C. Schlemminger, «Theoretical analysis of suitable fluids for high temperature heat pumps up to 125 °C heat delivery,» *International Journal of Refrigeration,* vol. 92, pp. 185-195, 2018. DOI: 10.1016/j.ijrefrig.2018.05.017

[14] L. Urbanucci, J. C. Bruno e D. Testi, «Thermodynamic and economic analysis of the integration of high-temperature heat pumps in trigeneration systems,» *Applied Energy,* vol. 238, pp. 516-533, 2019. DOI: 10.1016/j.apenergy.2019.01.115

[15] J. Choi, T. Kwak e Y. Yoo, «Cascade type heat pump system and control method thereof». South Korea Brevetto KR 101 236 603 B1, 22 02 2011.

[16] Y. Yerdesh, A. Toleukhanov, M. Mohanraj e O. Botella, «Air-to-Water Cascade Heat Pump Thermal Performance Modelling for Continental Climate Regions,» *Entropy: Thermodynamics – Energy – Environment – Economy,* vol. 3, n. 1, 2022. DOI: 10.21494/ISTE.OP.2022.0836

[17] H. W. Jung, H. Kang, W. J. Yoon e Y. Kim, «Performance comparison between a single-stage and a cascade multi-functional heat pump for both air heating and hot water supply,» *International Journal of Refrigeration,* vol. 36, n. 5, pp. 1431-1441, 2013. DOI: 10.1016/j.ijrefrig.2013.03.003

[18] S. Boahen e J. M. Choi, «A Study on the Performance of a Cascade Heat Pump for Generating Hot Water,» *Energies,* vol. 12, p. 4313, 2019. DOI: 10.3390/en12224313

[19] M. Yilmaz, «Performance analysis of a vapor compression heat pump using zeotropic refrigerant mixtures,» *Energy Conversion and Management,* vol. 44, pp. 267-282, 2003. DOI: 10.1016/S0196-8904(02)00054-7

[20] J. Navarro-Esbrí, Á. Fernández-Moreno e Á. Mota-Babiloni, «Modelling and evaluation of a high-temperature heat pump two-stage cascade with refrigerant mixtures as a fossil fuel boiler alternative for industry decarbonization,» *Energy,* vol. 254, n. B, 2022. DOI: 10.1016/j.energy.2022.124308

[21] K. Sezen e A. Gungor, «Comparison of solar assisted heat pump systems for heating residences: A review,» *Solar Energy,* vol. 249, pp. 424-445, 2023. DOI: 10.1016/j.solener.2022.11.051

[22] A.-G. Olabi, M. Mahmoud, K. Obaideen, E. T. Sayed, M. Ramadan e M. A. Abdelkareem, «Ground source heat pumps: Recent progress, applications, challenges, barriers, and role in achieving sustainable development goals based on bibliometric analysis,» *Thermal Science and Engineering Progress,* vol. 41, 2023. DOI: 10.1016/j.tsep.2023.101851

[23] R. Lazzarin e M. Noro, «Photovoltaic/Thermal (PV/T)/ground dual source heat pump: Optimum energy and economic sizing based on performance analysis,» *Energy and Buildings,* vol. 211, 2020. DOI: 10.1016/j.enbuild.2020.109800

[24] I. Staffell, D. Brett, N. Brandon e A. Hawkes, «A review of domestic heat pumps,» *Energy & Environmental Science,* vol. 5, n. 11, pp. 9291-9306, 2012. DOI: 10.1039/c2ee22653g

[25] K. Chua, S. Chou e W. Yang, «Advances in heat pump systems: A review,» *Applied Energy,* vol. 87, n. 12, pp. 3611-3624, 2010. DOI: 10.1016/j.apenergy.2010.06.014

[26] R. de Boer, A. Marina, B. Zühlsdorf, C. Arpagaus, M. Bantle, V. Wilk, B. Elmegaard, J. Corberán e J. Benson, «Strengthening Industrial Heat Pump Innovation,» 2020. [Online]. Available: https://www.sintef.no/en/publications/publication/1921809/. [Consultato il giorno 14 12 2023].

[27] I. Sarbu, Advances in Building Services Engineering, Cham, Switzerland: Springer, 2021. DOI: 10.1007/978-3-030-64781-0

[28] C. Arpagaus, F. Bless, M. Uhlmann, J. Schiffmann e S. S. Bertsch, «High temperature heat pumps: Market overview, state of the art, research status, refrigerants, and application potentials,» *Energy,* vol. 152, pp. 985-1010, 2018. DOI: 10.1016/j.energy.2018.03.166

[29] D. Bobelin, A. Bourig e J.-L. Peureux, «Experimental results of a newly developed very high temperature industrial heat pump (140°C) equipped with scroll compressors and working with a new blend refrigerant,» 2012.

[30] J. Stene, «Residential CO2 Heat Pump System fpr Combined Space Heating and Hot Water Heating,» 2004.

[31] J. Dhilipan, N. Vijayalakshmi, D. Shanmugam, R. J. Ganesh, S. Kodeeswaran e S. Muralidharan, «Performance and efficiency of different types of solar cell material – A review,» *Materials Today: Proceedings,* vol. 66, n. 3, pp. 1295-1302, 2022. DOI: 10.1016/j.matpr.2022.05.132

[32] S. Dubey, J. N. Sarvaiya e B. Seshadri, «Temperature Dependent Photovoltaic (PV) Efficiency and Its Effect on PV Production in the World - A Review,» *Energy Procedia,* vol. 33, pp. 311-321, 2013. DOI: 10.1016/j.egypro.2013.05.072

[33] C. Lamnatou e D. Chemisana, «Photovoltaic/thermal (PVT) systems: A review with emphasis on environmental issues,» *Renewable Energy,* vol. 105, pp. 270-287, 2017. DOI: 10.1016/j.renene.2016.12.009

[34] C. Ramos, A. Alcaso e A. Cardoso, «Photovoltaic-thermal (PVT) technology: Review and case study,» 2019. DOI: 10.1088/1755-1315/354/1/0120

[35] P. Sevela e B. W. Olesen, «Development and Benefits of Using PVT Compared to PV,» 2012.

[36] I. Sarbu e C. Sabarchievici, «A Comprehensive Review of Thermal Energy Storage,» *Sustainability,* vol. 191, n. 10, 2018. DOI: 10.3390/su10010191

[37] A. Schmidt, Technical Thermodynamics for Engineers Basics and Applications, Cham, Switzerland: Springer, 2019. DOI: 10.1007/978-3-030-20397-9

[38] F. Schmidt, «Large scale heat storage for district heating,» 2020.

[39] H.-J. Diersch e D. Bauer, «Analysis, modeling and simulation of underground thermal energy storage (UTES) systems,» in *Advances in Thermal Energy Storage Systems.*, Cambridge, UK, Elsevier, 2015, pp. 149-183. DOI: 10.1533/9781782420965.1.149

[40] Y. Dong, S. M. John e N. Lu, «Critical Review of Thermal Conductivity Models for Unsaturated Soils,» *Geotechnical and Geological Engineering,* vol. 33, n. 2, 2015. DOI: 10.1007/s10706-015-9843-2

[41] Meteonorm, «Meteonorm Version 8,» [Online]. Available: https://meteonorm.com/en/meteonorm-version-8. [Consultato il giorno 19 01 2024].

[42] E. Lemmon, I. Bell, M.Huber e M. McLinden, «REFPROP Documentation,» 21 05 2018. [Online]. Available: https://www.nist.gov/system/files/documents/2018/05/23/refprop10a.pdf. [Consultato il giorno 15 12 2023].

[43] R. Turton, R. C. Bailie, W. B. Whiting, J. A. Schaeiwitz e D. Bhattacharyya, Analysis, Systesis and Design of Chemical Processes, Ann Arbor MI, USA: Prentice Hall, 2012. ISBN 13: 978-0-13-261812-0

[44] J. Sarkar e S. Bhattacharyya, «Assessment of blends of CO2 with butane and isobutane as working fluids for heat pump applications,» *International Journal of Thermal Sciences,* vol. 48, pp. 1460-1465, 2009. DOI: 10.1016/j.ijthermalsci.2008.12.002

[45] G. Towler e R. Sinnott, Chemical Engineering Design - Principles, Practice and Economics of Plant and Process Desing, Burlington MA, USA: Elsevier, 2008. ISBN 13: 978-0-7506-8423-1

[46] M. Herrando, A. Ramos, I. Zabalza e C. N. Markides, «A comprehensive assessment of alternative absorber-exchanger design for hybrid PVT-water collectors,» *Applied Energy,* vol. 235, pp. 1583-1602, 2019. DOI: 10.1016/j.apenergy.2018.11.024

[47] Dannevig e Hartsveit, «Klima i Norge,» Store Norske Leksikon, 28 10 2022. [Online]. Available: https://snl.no/klima_i_Norge#-Middeltemperaturer_(%C2%B0C)_i_Norge. [Consultato il giorno 15 12 2023].

[48] P. J. Michaels, R. C. Balling Jr, R. S. Vose e P. C. Knappenberger, «Analysis of trends in the variability of daily and monthly historical temperature measurements,» *Climate Research,* vol. 10, pp. 27-33, 1998.

[49] N. K. Noyanbayev, A. J. Forsyth e T. Feehally, «Efficiency analysis for a grid-connected battery energy storage system,» *Materials Today Proceedings,* vol. 5, n. 11, pp. 22811-22818, 2018. DOI: 10.1016/j.matpr.2018.07.095